

Quadrupolar NMR Relaxation as a Local Probe of Collective Dynamics in Aqueous Alkaline and Alkaline-Earth Chlorides Solutions

Matthieu Wolf,¹ Iurii Chubak,¹ and Benjamin Rotenberg^{1,2}

¹*Sorbonne Université, CNRS, Physicochimie des Électrolytes et Nanosystèmes Interfaciaux, F-75005 Paris, France*

²*Réseau sur le Stockage Electrochimique de l'Énergie (RS2E), FR CNRS 3459, 80039 Amiens Cedex,^a France*

(Dated: 11 February 2025)

While nuclear magnetic resonance (NMR) provides valuable insights into the local environment of many nuclei, the unambiguous interpretation of the signal in terms of microscopic dynamics is often difficult, particularly when the quadrupolar relaxation mechanism comes into play. Here, we investigate the quadrupolar NMR relaxation of cations and anions in aqueous alkaline and alkaline-earth chlorides solutions, across a broad range of salt concentrations. Using a combination of DFT calculations and classical molecular dynamics simulations, we compute the electric field gradient (EFG) fluctuations over the relevant time scales. Predicted NMR relaxation rates are in good agreement with experiments from the literature. As previously reported for NaCl, we find that the increase in relaxation rate with salt concentration is primarily driven by the slowing of EFG fluctuations, while changes in the static variance of the EFG play a minor role. We highlight some specific features for smaller and divalent cations compared to the other monovalent ones. Additionally, we assess the relevance of the Stokes-Einstein-Debye model, frequently used to analyze NMR relaxation experiments, for these aqueous electrolytes, and highlight the link between the collective dynamics of the liquid underlying the EFG fluctuations at the ion positions and the stress fluctuations. Our results generalize observations for Na⁺ in aqueous NaCl solutions, showing that models assuming a viscous model of the solvent dynamics are insufficient to describe EFG fluctuations in these systems and illustrate the relevance of molecular simulations to interpret NMR relaxation experiments in terms of microscopic dynamics.

^a)Electronic mail: benjamin.rotenberg@sorbonne-universite.fr

I. INTRODUCTION

Detailed information on the solvation shell structure and dynamics of aqueous alkaline and alkaline-earth cations can shed light on multiple technological, chemical, and biological phenomena¹⁻⁵. While nuclear magnetic resonance (NMR) can provide valuable insights on chemical arrangements and relaxation in the environment of many nuclei, the unambiguous interpretation of the signal is often hindered when the quadrupolar relaxation mechanism comes into play. The latter applies to nuclei with spin $I \geq 1$ (such as ${}^7\text{Li}^+$, ${}^{23}\text{Na}^+$, ${}^{39}\text{K}^+$, ${}^{25}\text{Mg}^{2+}$, ${}^{43}\text{Ca}^{2+}$, ${}^{133}\text{Cs}^+$, ${}^{85}\text{Rb}^+$, etc), for which the main interaction is that between the nuclear quadrupolar moment eQ and the electric field gradient (EFG) tensor at its position⁶.

The strength of the quadrupolar interaction together with thermal fluctuations of molecular environments of the nucleus (having a characteristic correlation time τ_c) govern the relaxation of the distribution of nuclear spins in the external static magnetic field B_0 towards equilibrium⁶. Assuming that molecular processes are sufficiently fast, *i.e* a Larmor frequency $\gamma_n B_0 \ll \tau_c^{-1}$ with γ_n the nuclear gyromagnetic ratio (so-called extreme narrowing regime), the spin-lattice $1/T_1$ and spin-spin $1/T_2$ rates describing the magnetization relaxation along the longitudinal and transverse directions with respect to B_0 , respectively, become equal. They further read^{6,7}:

$$\frac{1}{T_1} = \frac{1}{T_2} = \frac{1}{20} \frac{2I + 3}{I^2(2I - 1)} \left(\frac{eQ}{\hbar} \right)^2 \int_0^\infty dt \langle \mathbf{V}(t) : \mathbf{V}(0) \rangle, \quad (1)$$

where \mathbf{V} is the full EFG tensor at the nucleus that includes the electronic cloud contribution, $C_{\text{EFG}}(t) \equiv \langle \mathbf{V}(t) : \mathbf{V}(0) \rangle = \left\langle \sum_{\alpha, \beta} V_{\alpha\beta}(t) V_{\alpha\beta}(0) \right\rangle$ ($\alpha, \beta = x, y, z$) is the EFG autocorrelation function (ACF), and \hbar stands for the reduced Planck constant. This expression, obtained within linear response theory, allows to predict the relaxation time from equilibrium simulations in the absence of applied magnetic field: $\langle \dots \rangle$ denotes an average in the canonical ensemble, with fixed number of particles N , system volume V and temperature T .

While quadrupolar NMR relaxation rates (1) can elucidate the structure and dynamics of ionic solvation shells, the interpretation of experimental data is often challenging due to the limited knowledge of quadrupolar coupling constants and of molecular mechanisms behind relaxation. A series of models have thus been proposed to rationalize the observations. Hynes and Wolynes developed an analytical theory based on the quadrupole reorientation dynamics in a continuous dielectric solvent⁸. Perng and Ladanyi dropped the continuous

solvent description in their refined dielectric theory coupling the field gradient dynamics to solvent charge density fluctuations⁹. While the continuous dielectric theory of Hynes and Wolynes⁸ typically underestimated the predicted values of the quadrupolar rates, the theory of Perng and Ladanyi⁹ was able to achieve quantitative agreement with experiments, yet it relied on a free parameter. Bosse *et al.* formulated a mode-coupling theory for the EFG relaxation in molten salts¹⁰. A series of models by Hertz *et al.* related the correlation time of EFG fluctuations to water dipole reorientation^{11–13}. However, this molecular mechanism was shown to oversimplify many-body correlations in the context of quadrupolar relaxation dynamics^{7,14,15}. More recently, the EFG correlation time was suggested to be interpreted as the rotational correlation time for an object in a continuous solvent^{16–18}, likely to be associated with collective stochastic rotations of the ionic solvation shell^{19,20}. While rotational diffusion is clearly at play in the case of *intramolecular* quadrupolar relaxation²¹, as for the relaxation of ²H in heavy water, its applicability to the problem of single quadrupolar ions that is inherently *intermolecular* requires a thorough investigation.

The predictions of the above-mentioned theories have been tested both with *ab initio*^{22–26} and classical^{7,15,27–34} MD simulations. In particular, the isotropic monoexponential character of the quadrupolar relaxation dynamics that is often assumed in theories with a continuous solvent description was challenged both at the *ab initio* and classical levels. Using classical MD, Roberts and Schnitker⁷ highlighted a pronounced effect of intermolecular cross correlations on the EFG relaxation that are treated in a rather simplified fashion within molecular dipole reorientation models^{11–13}. Carof *et al.*¹⁵ underlined a major role of collective fluctuations in ionic solvation shells on the EFG dynamics.

Compared to classical MD approaches that rely on the Sternheimer approximation for the electron cloud contribution to the EFG at the ion position^{30,33–36}, *ab initio* methods, in particular those relying on density functional theory (DFT) calculations³⁷, provide a very good accuracy of the computed EFGs^{22,24,26,37–39}. Nevertheless, the high cost of such simulations limits the sampling of the EFG fluctuations^{22–24} over the time scales necessary to precisely compute the integral in Eq. (1). Therefore, on one hand, the use of the fully first-principles approach may not be appropriate in concentrated electrolyte solutions considered here, for which the quadrupolar NMR relaxation slows down with increasing salt concentration and decreasing temperature^{11–13,19,20,34}. On the other hand, the Sternheimer factors used in classical MD approaches were shown to be sensitive to the local charge distribution around the

ion generated with a specific force field at hand^{30,33}, and their concentration dependence might be necessary to be taken into account³⁴. Thus, while classical MD offers a better precision in determining the statistical relaxation of the field gradient fluctuations, it must be coupled with pertinent estimates of the Sternheimer factors to describe local chemical environments.

Here, building on our previously developed strategy, we combine DFT calculations with classical molecular dynamics simulations to investigate the concentration dependence of the quadrupolar NMR relaxation rates of ions in aqueous alkaline and alkaline-earth chloride solutions and their relation to solution viscosity. The systems and methods are presented in Section II, while results are shown and discussed in Section III.

II. SYSTEM AND METHODS

A. Molecular dynamics

We performed classical molecular dynamics simulations of a set of aqueous electrolyte solutions (LiCl, NaCl, KCl, RbCl, CsCl, MgCl₂ and CaCl₂) at salt molalities ranging from $c = 0.06$ to 4 m, with LiCl extended up to 10 m, using the Madrid-2019 force field^{40,41}, which incorporates scaled ionic charges and the rigid four-site TIP4P/2005 water model⁴². All interactions are described as

$$U_{\text{tot}}^{\text{Madrid-2019}} = U_{\text{el}} + U_{\text{LJ}}, \quad (2)$$

where U_{el} denotes the electrostatic Coulomb potential between two point charges q^i and q^j at a distance r_{ij}

$$U_{\text{el}} = \sum_{i < j} \frac{q^i q^j}{4\pi\epsilon_0 r_{ij}}, \quad (3)$$

with ϵ_0 the vacuum permittivity, and U_{LJ} describes short-range Lennard-Jones interactions

$$U_{\text{LJ}} = \sum_{i < j} 4\epsilon_{ij} \left[\left(\frac{\sigma_{ij}}{r_{ij}} \right)^{12} - \left(\frac{\sigma_{ij}}{r_{ij}} \right)^6 \right]. \quad (4)$$

As a mean-field, effective inclusion of the electronic polarizability of the medium⁴³, the ions carry scaled charges $\pm 0.85e$ (monovalent cations and anions) and $+1.70e$ (divalent cations) with e the elementary charge. The water molecules carry partial charges $q_{\text{H}} = +0.5564e$,

$q_{\text{O}} = 0$, $q_{\text{M}} = -2q_{\text{H}}$ (the virtual M-site lies along the HOH vector bisector). All the relevant Lennard-Jones interaction parameters ϵ_{ij} and σ_{ij} were taken from Refs. 40,41.

Similarly to our previous work³⁴ on the case of NaCl (whose results are reused in the present work for comparison with the other ions), $N = 1000$ water molecules N_{p} ion pairs were initialized in a cubic box at the equilibrium solution density $\rho(c, T)$ obtained with NPT simulations at $P = 1$ bar and $T = 298.15$ K. The resulting densities are in very good agreement with the experimental ones, as discussed in Refs. 40,41. The production runs were done in the NVT ensemble. All simulations were carried out with the open-source MetalWalls package^{44,45} on graphics processing units with electrostatic interactions computed with Ewald summation⁴⁶ and a short-range cutoff of 1.24 nm, using the velocity Verlet algorithm with a time step of 1 fs and a Nosé-Hoover chain thermostat with a time constant of 1 ps. Water molecules are treated as rigid using the RATTLE algorithm with a precision of 10^{-9} . For each system, five independent runs of 5 ns were performed to sample (every 50 fs) the EFG at the ion positions. The EFG was computed on these configurations using full Ewald summations⁴⁶ implemented in MetalWalls³³.

B. Sternheimer approximation

We employ the Sternheimer approximation³⁵, in which a linear relation between the total EFG tensor \mathbf{V} at the nucleus and the external EFG \mathbf{V}^{ext} is assumed, $\mathbf{V} \simeq (1 + \gamma)\mathbf{V}^{\text{ext}}$, with γ being the Sternheimer (anti-)shielding factor^{36,47}. Specifically, it is assumed that the electronic cloud contribution to the EFG amplifies the field gradient induced by the surrounding charge distribution, yielding values of γ that are typically large^{30,33,36,47}. The quadrupolar relaxation rate in Eq. (1) can thus be rewritten as

$$\frac{1}{T_1} = C_Q(1 + \gamma)^2 \langle \mathbf{V}_{\text{ext}}^2 \rangle \tau_c, \quad (5)$$

with the constant $C_Q \equiv \frac{1}{20} \frac{2I+3}{I^2(2I-1)} \left(\frac{eQ}{\hbar}\right)^2$, the external EFG variance $\langle \mathbf{V}_{\text{ext}}^2 \rangle \equiv \langle \mathbf{V}_{\text{ext}}(0) : \mathbf{V}_{\text{ext}}(0) \rangle$, and the correlation time τ_c

$$\tau_c = \langle \mathbf{V}_{\text{ext}}^2 \rangle^{-1} \int_0^\infty dt \langle \mathbf{V}_{\text{ext}}(t) : \mathbf{V}_{\text{ext}}(0) \rangle. \quad (6)$$

The electric field gradient \mathbf{V}_{ext} arising from the external charge distribution surrounding an ion is generally unknown. Here, we approximate it using the point charge distribution

induced by the employed classical force field^{30,33}. To relate this force-field-based \mathbf{V}_{ext} to the total EFG, \mathbf{V}_{AI} , which can be obtained from ab initio calculations, we introduce the effective Sternheimer factor γ_{eff} . This factor is determined for a given nucleus by correlating \mathbf{V}_{AI} with \mathbf{V}_{ext} on the same set of configurations of the aqueous solution^{30,33}. The Sternheimer factors at infinite dilution γ_{eff} were previously calculated for Li^+ , Na^+ , K^+ , Cl^- , Mg^{2+} , and Ca^{2+} ions by comparing the classical \mathbf{V}_{ext} and ab initio \mathbf{V}_{AI} values of the EFG at the ion position, using configurations generated with the Madrid-2019 force field^{40,41}, as detailed in Ref. 33.

At that time, however, the Rb^+ and Cs^+ ions were not yet included in the Madrid-2019 force field, so the corresponding effective Sternheimer factors could not be determined. In 2022, the Madrid-2019 force field was extended⁴¹ to include Rb^+ and Cs^+ , allowing us to compute their Sternheimer factors for this force field. Thus, to evaluate the validity of the Sternheimer approximation and determine the corresponding γ_{eff} for Rb^+ and Cs^+ , we followed the same methodology as in Ref. 33 by comparing the cartesian components of the EFG tensor obtained from classical molecular dynamics simulations, $\mathbf{V}_{\alpha\beta}^{\text{ext}}$, with those obtained from electronic DFT calculations, $\mathbf{V}_{\alpha\beta}^{\text{AI}}$. For each ion, we performed five independent classical MD simulations, using the Madrid-2019 force field, of a small system consisting of 64 water molecules and a single ion. The initial configurations were prepared following the same procedure as mentioned above for the larger systems. For the five independent systems, we sampled 1000 configurations every 10 ps during a single *NVT* production run. These configurations were then used as input for the DFT-based computations of the EFG in the condensed phase, which includes the electronic contributions. The ab initio calculations were performed using the Quantum Espresso (QE) package with the projector augmented wave (PAW) method⁴⁸, which allows for a more accurate representation of the core region. The Perdew-Burke-Ernzerhof (PBE) functional was employed, with a kinetic energy cutoff of 80 Ry. Additionally, it is important to note that the GIPAW pseudopotentials⁴⁹ commonly used for NMR investigations were not available for Rb^+ and Cs^+ so that we used the KJPAW⁵⁰ pseudopotentials for these two ions.

In Ref. 34, we showed that for Na^+ the Sternheimer factor only slightly depends on the salt concentration in solution (likely due to modifications in the ionic hydration shell), and that one could obtain sufficiently accurate predictions using the value at infinite dilution. Furthermore, we observed in this case that the classical EFG tends to underestimate the ab initio value \mathbf{V}_{AI} by more than 20%. For more accurate predictions of the EFG variance,

we introduce a modified Sternheimer factor, γ'_{eff} , such that $(1 + \gamma'_{\text{eff}})^2 = \langle \mathbf{V}_{\text{AI}}^2 \rangle / \langle \mathbf{V}_{\text{ext}}^2 \rangle$, using the values of $\langle \mathbf{V}_{\text{AI}}^2 \rangle$ and $\langle \mathbf{V}_{\text{ext}}^2 \rangle$, resulting in an EFG variance prediction within 5% accuracy. Thus, for all the ions considered in the present work, we estimated γ'_{eff} using the ratio $\langle \mathbf{V}_{\text{AI}}^2 \rangle / \langle \mathbf{V}_{\text{ext}}^2 \rangle$ from the data available in Ref. 33, except for Rb^+ and Cs^+ , for which we used the new data obtained here. The Sternheimer factors γ_{eff} and γ'_{eff} for all ions are presented in Section II B.

C. Dynamical properties

The EFG autocorrelation function $C_{\text{EFG}}(t)$ is computed from the components $V_{\alpha\beta}(t)$ sampled every 50 fs of the larger systems described in Section II A. In order to link the quadrupolar NMR relaxation with the dynamics of the electrolyte solution, for each salt and concentration, we consider the viscosity and ion diffusion coefficients. The shear viscosity is computed from the Green-Kubo relation⁵¹:

$$\eta = \frac{V}{k_{\text{B}}T} \int_0^{+\infty} dt C_{\text{stress}}(t), \quad (7)$$

with V the volume, k_{B} the Boltzmann constant, and $C_{\text{stress}}(t)$ the ACF of the symmetrized and traceless stress tensor $P_{\alpha\beta}$ ⁵¹:

$$C_{\text{stress}}(t) = \frac{1}{10} \sum_{\alpha,\beta} \langle P_{\alpha\beta}(t) P_{\alpha\beta}(0) \rangle, \quad (8)$$

where α, β run over the three Cartesian components and $P_{\alpha\beta} = \frac{1}{2}(\sigma_{\alpha\beta} + \sigma_{\beta\alpha}) - \frac{1}{3}\delta_{\alpha\beta} \sum_{\gamma} \sigma_{\gamma\gamma}$. The stress tensor $\sigma_{\alpha\beta}$ is sampled every step of the MD trajectory (1 fs). The diffusion coefficients are obtained from the long time limit of the mean-square displacements:

$$D = \lim_{t \rightarrow \infty} \frac{1}{6Mt} \sum_{i=1}^M \langle [\mathbf{r}_i(t) - \mathbf{r}_i(0)]^2 \rangle, \quad (9)$$

where M is the number of ions or water molecules, $\mathbf{r}_i(t)$ is the i -th particle position at time t , and the brackets $\langle \dots \rangle$ denote ensemble averaging. We apply the Yeh-Hummer relation⁵² to account for the finite simulation box size:

$$D_{\infty} = D + \frac{k_{\text{B}}T\xi}{6\pi\eta L} \quad (10)$$

with D_{∞} corresponding to the diffusion coefficient in a macroscopic system, D that in a cubic simulation box with side length L , and $\xi \approx 2.837297$. The finite-size correction amounted to around 20% of the measured value D .

Within the Stokes-Einstein-Debye (SED) model^{53,54}, the time scale of EFG fluctuations is obtained as:

$$\tau_c^{\text{SED}} = \frac{4\pi\eta r_0^3}{3k_B T}, \quad (11)$$

where η is the dynamics viscosity of the medium and r_0 is the ion's hydrodynamic radius obtained using the Stokes-Einstein relation:

$$r_0 = \frac{k_B T}{6\pi\eta D}. \quad (12)$$

III. RESULTS AND DISCUSSION

A. Sternheimer approximation for Rb^+ and Cs^+

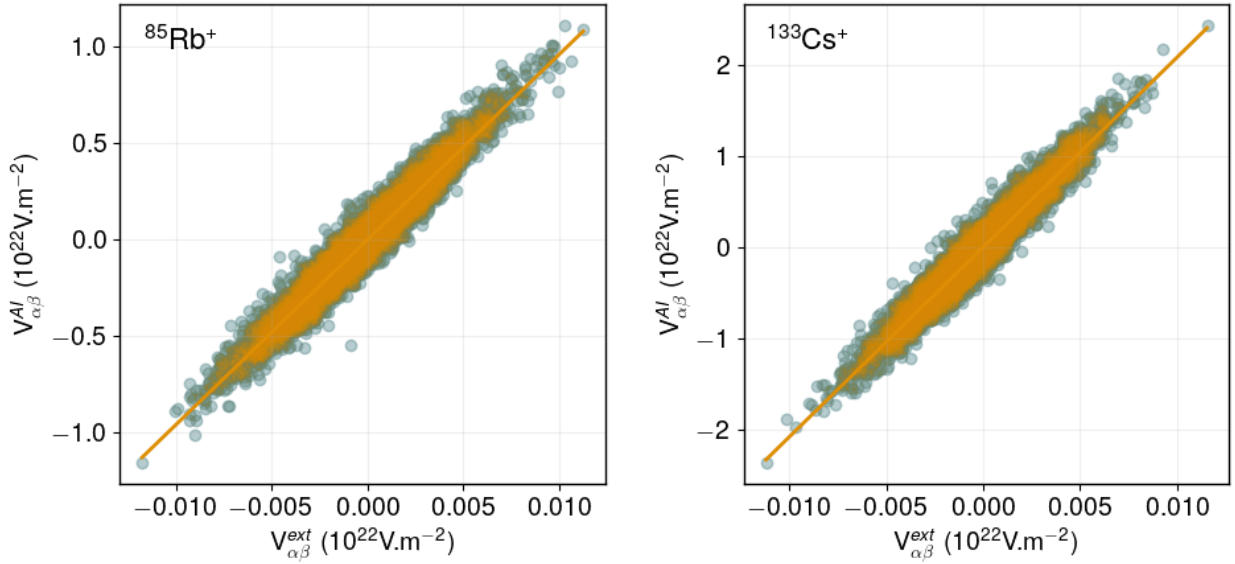


FIG. 1. Comparison between the ab initio EFG components, $V_{\alpha\beta}^{\text{AI}}$, (computed using the QE-KJPAW package) and the classical ones from the Madrid-2019 force field, $V_{\alpha\beta}^{\text{ext}}$, at the position of Rb^+ and Cs^+ ions at infinite dilution in water. The colors correspond to 2 sets of 1000 configurations from 2 independent MD simulations. In each panel, the solid line indicates the linear fit $V_{\alpha\beta}^{\text{AI}} = (1 + \gamma_{\text{eff}}) V_{\alpha\beta}^{\text{ext}}$.

Fig. 1 shows the components of the EFG tensor computed from DFT calculations, $V_{\alpha\beta}^{\text{AI}}$, as a function of the ones computed with the Madrid-2019 force field, $V_{\alpha\beta}^{\text{ext}}$, for aqueous Rb^+ and Cs^+ ions. In each case, results are shown only for 2 of the 5 sets of 1000 configurations

for clarity. The correlation between the classical and ab initio results is comparable to that obtained with other ions (see Ref. 33). It confirms the relevance of the Sternheimer approximation for these ions, and that the variance $\langle \mathbf{V}_{\text{AI}}^2 \rangle$ is underestimated by $(1 + \gamma_{\text{eff}})^2 \langle \mathbf{V}_{\text{ext}}^2 \rangle$, due to the spread around the linear correlation. As explained in Section II B, we therefore define a modified Sternheimer factor as $(1 + \gamma'_{\text{eff}})^2 = \langle \mathbf{V}_{\text{AI}}^2 \rangle / \langle \mathbf{V}_{\text{ext}}^2 \rangle$. Since this was not previously done, we also computed the same quantity for the other ions using the data available in Ref. 33. All the Sternheimer and modified Sternheimer factors corresponding to the Madrid-2019 force field are summarized in Table I.

Ion	γ_{eff}	γ'_{eff}
Li ⁺	0.362 ± 0.01	0.42 ± 0.02
Na ⁺	10.54 ± 0.11	12.09 ± 0.14
K ⁺	28.51 ± 0.33	34.57 ± 0.43
Rb ⁺	94.57 ± 0.34	97.35 ± 0.36
Cs ⁺	207.05 ± 0.76	213.71 ± 0.76
Mg ²⁺	18.34 ± 0.17	20.56 ± 0.33
Ca ²⁺	36.24 ± 0.30	39.54 ± 0.59
Cl ⁻	20.25 ± 0.22	23.52 ± 0.03

TABLE I. Effective Sternheimer factors (γ_{eff}) and modified Sternheimer factors (γ'_{eff}), for different ions at infinite dilution in TIP4P/2005 water. The values for Li⁺, Na⁺, K⁺, Cl⁻, Mg²⁺, and Ca²⁺ were obtained (directly for γ_{eff} , and as described in the text for γ'_{eff}) from our previous studies^{33,34}, while those for Rb⁺ and Cs⁺ were computed in this work.

The values of γ'_{eff} are slightly larger by $12 \pm 6\%$ than γ_{eff} , consistently with the underestimation of the variance by the usual Sternheimer approximation. Both γ_{eff} and γ'_{eff} increase when increasing the number of electrons in the ion (from Li⁺ to Cs⁺ and from Mg²⁺ to Ca²⁺), reflecting the larger response of the ionic cloud to an external perturbation. We also note that for isoelectronic ions (Na⁺ and Mg²⁺; Cl⁻, K⁺ and Ca²⁺) both γ_{eff} and γ'_{eff} increase when increasing the charge of the nucleus.

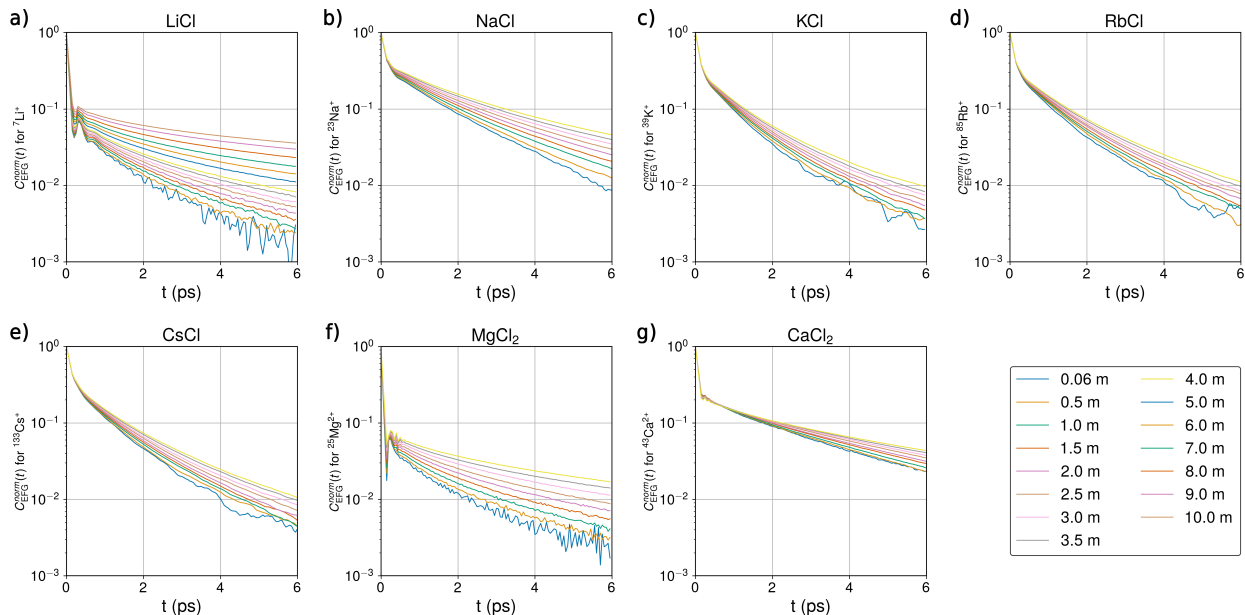


FIG. 2. Normalized autocorrelation function of the electric field gradient at the cation position in aqueous solutions of (a) LiCl, (b) NaCl, (c) KCl, (d) RbCl, (e) CsCl, (f) MgCl₂, and (g) CaCl₂ as a function of time, presented for various molalities indicated by the line colors.

B. Relaxation of electric field gradient fluctuations

The normalized ACF of the classical ACF, $C_{\text{EFG}}^{\text{norm}}(t)$, is reported for all cations in Fig. 2. Each panel corresponds to a given salt and the color of the lines indicates the molality. All results exhibit similar trends with time and concentration: an initial rapid decay occurring over the first 0.2 ps that is relatively independent of concentration, as shown more precisely in Fig. S1 of the Supplementary Information (SI), followed by a slower decay (over several ps), which depends significantly on the salt concentration. For the lighter cations Li⁺ and Mg²⁺ (and to a lesser extent Ca²⁺), one can also observe an intermediate oscillatory regime, due to their tight confinement within the solvation shell³¹.

Increasing the salt concentration slows down the decay of the cation EFG ACF for all cations, as already observed for NaCl in Ref. 34. Such a slowdown is more pronounced for LiCl and MgCl₂. This effect is likely related to their small ionic radii⁵⁵ and the well-organized hydration shells that they form^{56,57}. Even though the hydration shell of CaCl₂ is similar to that of MgCl₂ in terms of hydration numbers⁵⁸, Fig. 2g indicates that, within the 0 to 6 ps range, the salt concentration has a very limited effect on the slow relaxation mode

of CaCl_2 . However, its effect is visible on longer time scales, as shown in SI Fig. S2, which compares $C_{\text{EFG}}^{\text{norm}}(t)$ at the cation positions for aqueous MgCl_2 and CaCl_2 . The two systems exhibit similar behaviors, with differences arising from the larger size of Ca^{2+} , leading to a less structured hydration shell (also reflected in the larger variance of the EFG³³). This analysis emphasizes the necessity of long-time sampling of the EFG to accurately determine the decorrelation time τ_c , hence the relaxation rate $1/T_1$.

Similarly, for chloride ions across all seven systems, as shown in SI Figs. S3 and S4, $C_{\text{EFG}}^{\text{norm}}(t)$ displays comparable behavior, with an initial rapid decay followed by much slower secondary decays. Interestingly, the intermediate oscillatory regime observed for Li^+ , Mg^{2+} and Ca^{2+} is barely visible for Cl^- in the corresponding salt, supporting the above-mentioned interpretation as resulting from the tight solvation shell around these cations. Increasing the salt concentration induces a slowdown in the decay of $C_{\text{EFG}}^{\text{norm}}(t)$ at the anion positions for all systems. However, this effect is more pronounced in aqueous chloride solutions with divalent cations, MgCl_2 and CaCl_2 , suggesting again the possible role of ion pairs in these systems.

In order to quantify the decay of the normalized EFG ACF of cations and anions in the seven considered electrolytes, following Ref. 34 for Na^+ in aqueous NaCl we model the MD results for $C_{\text{EFG}}^{\text{norm}}(t)$ by a fit of the form:

$$f(t) = (1 - \alpha_s)e^{-t/\tau_f} + \alpha_s e^{-[t/\tau_s]^\beta} \quad (13)$$

where the first exponential term describes the fast initial decay, with characteristic time τ_f never exceeding 0.12 ps, and the second stretched exponential describes the slower decay with relative weight α_s . In practice, we first obtain τ_f for each case assuming $\beta = 1$ and fitting the data to Eq. 13 only for $t < 1$ ps. We then fix the value of τ_f for the rest of the procedure. For each salt, we then fit the three remaining parameters (β, τ_s, α_s) using the MD results only for $t > 1$ ps, for a molality 0.5 m. The optimal values of β for cations (resp. anions) across all seven electrolytes yielded a mean value of $\beta \approx 0.59 \pm 0.11$ (resp. $\beta \approx 0.65 \pm 0.11$), which suggests a broad distribution of relaxation modes. The values for each salt are provided in SI Table II. The values of β obtained at 0.5 m are then used for all other molalities of the same salt, and only τ_s and α_s are fitted. The fits to Eq. 13, shown for all salts in SI Figures S5 and S6, describe the MD results very well. Moreover, by integrating Eq. 13 for all the cations and anions (see Figs. S7 and S8), we find that for all systems, the

slow decay provides the main contribution to the overall EFG decorrelation time τ_c obtained by integrating $C_{\text{EFG}}^{\text{norm}}(t)$, suggesting a broad distribution of relaxation modes in the overall EFG relaxation.

C. Quadrupolar NMR relaxation rates

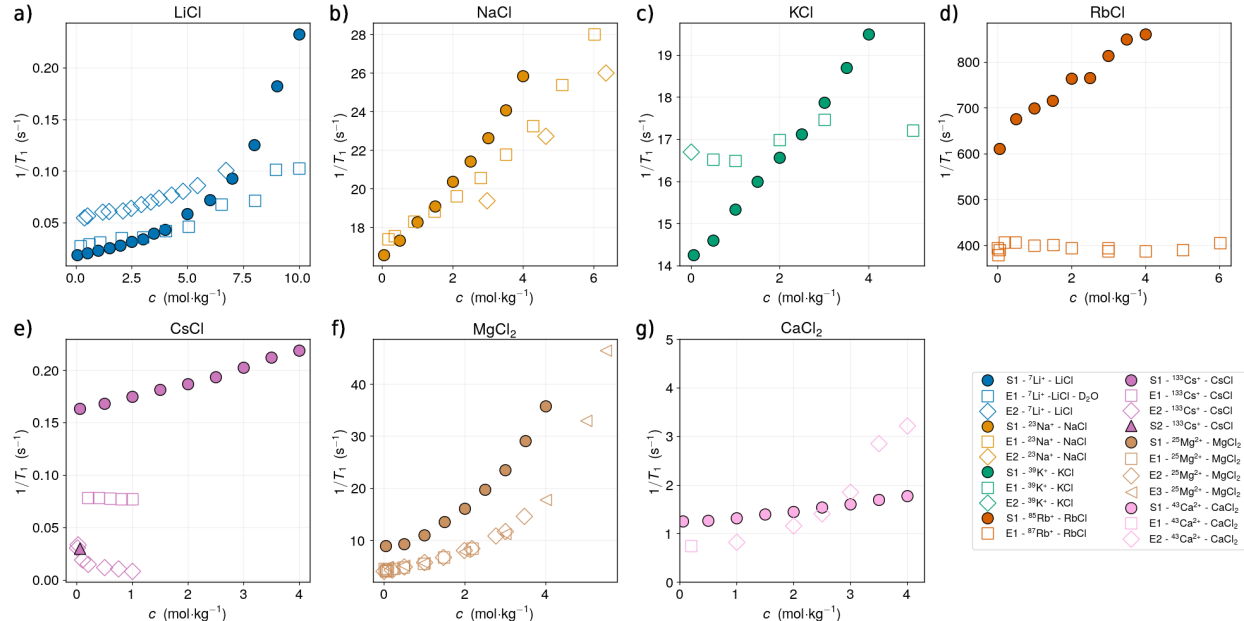


FIG. 3. NMR relaxation rates as a function of the molality for six different ions ${}^7\text{Li}^+$, ${}^{23}\text{Na}^+$, ${}^{39}\text{K}^+$, ${}^{85}\text{Rb}^+$ (${}^{87}\text{Rb}^+$ for experimental results), ${}^{133}\text{Cs}^+$, ${}^{25}\text{Mg}^{2+}$ and ${}^{43}\text{Ca}^{2+}$ in seven different aqueous systems: (a) LiCl, (b) NaCl, (c) KCl, (d) RbCl, (e) CsCl, (f) MgCl_2 , and (g) CaCl_2 . The values are compared to experimental values, with the following references: for Li^{32,59}, Na^{34,60}, K^{61,62}, Rb⁶³, Cs^{62,64,65}, Ca^{66,67}, Mg^{64,68,69}.

Figure 3 compares the quadrupolar NMR relaxation rates computed by Eq. (5) as described above (full symbols) with that measured experimentally (open symbols). All the corresponding simulation data is available in SI Table III. As shown in SI Fig. S9, the convergence of the integral to compute the EFG correlation time τ_c (see Eq. 6) necessitates a good estimate of the normalized EFG ACF over times longer than 30 ps for the slowest decaying cases, in particular at high concentrations. This requires sampling long trajectories (several ns), which cannot be achieved with ab initio MD. However, the combination of classical MD with the effect of the electron cloud contribution via DFT calculations and the

modified Sternheimer approximation provides a good estimate with experimental relaxation rates.

The NMR relaxation rates $1/T_1$ obtained from our simulations (S1 in Fig. 3) are of the same order of magnitude as the corresponding experimental results (E1 and E2 in Fig. 3) for all cations. Additionally, at a molality of 2 m, we find the following order for the relaxation rates $1/T_1$ across different cations: ${}^7\text{Li}^+$ (0.028 s^{-1}) $<$ ${}^{133}\text{Cs}^+$ (0.1868 s^{-1}) $<$ ${}^{43}\text{Ca}^{2+}$ (1.4480 s^{-1}) $<$ ${}^{25}\text{Mg}^{2+}$ (16.11 s^{-1}) $<$ ${}^{39}\text{K}^+$ (16.57 s^{-1}) $<$ ${}^{23}\text{Na}^+$ (20.38 s^{-1}) $<$ ${}^{87}\text{Rb}^+$ (763.96 s^{-1}), which matches perfectly the order of the experimental values available at 2m: ${}^7\text{Li}^+$ (0.062 s^{-1}) $<$ ${}^{43}\text{Ca}^{2+}$ (1.16 s^{-1}) $<$ ${}^{25}\text{Mg}^{2+}$ (8 s^{-1}) $<$ ${}^{39}\text{K}^+$ (17 s^{-1}) $<$ ${}^{23}\text{Na}^+$ (19.63 s^{-1}) $<$ ${}^{87}\text{Rb}^+$ (393.9 s^{-1}). Similarly, at a higher molality of 4 m, the relaxation rates $1/T_1$ for the cations from our simulations closely follow the order observed in experimental data, except for ${}^{25}\text{Mg}^{2+}$, for which we predict a $1/T_1$ larger than that of ${}^{23}\text{Na}^+$, while the opposite is seen in the experimental results. Overall, the NMR relaxation rates at 4 m are ranked as follows for the simulation data: ${}^7\text{Li}^+$ (0.0433 s^{-1}) $<$ ${}^{133}\text{Cs}^+$ (0.2189 s^{-1}) $<$ ${}^{43}\text{Ca}^{2+}$ (1.7710 s^{-1}) $<$ ${}^{39}\text{K}^+$ (19.49 s^{-1}) $<$ ${}^{23}\text{Na}^+$ (25.85 s^{-1}) $<$ ${}^{25}\text{Mg}^{2+}$ (35.74 s^{-1}) $<$ ${}^{87}\text{Rb}^+$ (860.74 s^{-1}), and for the experimental values: ${}^7\text{Li}^+$ (0.077 s^{-1}) $<$ ${}^{43}\text{Ca}^{2+}$ (3.226 s^{-1}) $<$ ${}^{39}\text{K}^+$ (17.21 s^{-1}) $<$ ${}^{25}\text{Mg}^{2+}$ (17.8 s^{-1}) $<$ ${}^{23}\text{Na}^+$ (23 s^{-1}) $<$ ${}^{87}\text{Rb}^+$ (387.59 s^{-1}).

For the first two systems, LiCl and NaCl, the behaviour of the evolution of the NMR relaxation rates from our simulations is in very good agreement with the experimental data, particularly within the concentration ranges $0 \text{ m} < c < 7 \text{ m}$ for LiCl and $0 \text{ m} < c < 3.5 \text{ m}$ for NaCl. For LiCl, the simulation results closely match the NMR relaxation data for ${}^7\text{Li}^+$ in D_2O up to 6 m, with a relative error of smaller than 20%. As expected, the experimental rates for ${}^7\text{Li}^+$ in H_2O are larger, due to the additional contribution of dipolar relaxation induced by the water hydrogen spins. Therefore, the better agreement between our predicted rate at 7 m and the experimental results in H_2O than in D_2O is fortuitous. For NaCl, deviations appear around 3.5 m, after which the simulation data slightly overestimate the experimental values. However, even at 4 m, the relative error is only $\approx 13\%$. Moreover, as mentioned in our previous study on NaCl only³⁴, this overestimation is likely due to limitations of the employed force field in capturing the dynamic properties of solutions at higher molality, and we expect the same origin for the other salts considered in the present work. For KCl, the simulations match the experimental values closely between $1.5 \text{ m} < c < 3 \text{ m}$, with a relative error below 10%. Above 3.5 m (resp. below 1 m), the simulations tend to overestimate

(resp. underestimate) $1/T_1$. Nonetheless, at 0.5 m and 4 m, the relative error is $\lesssim 13\%$.

For the other alkaline chlorides, RbCl and CsCl, our simulation results are generally of the same order of magnitude as the experimental data. For CsCl, the simulations exhibit a behavior consistent with experimental observations over the small range of available data. However, for both systems the simulations tend to overestimate the NMR relaxation rates, yielding values approximately 1.6 to 2.2 times larger than the experimental results, depending on the salt concentration. In the RbCl case, this overestimation could be influenced by the differences between the isotopes $^{85}\text{Rb}^+$ and $^{87}\text{Rb}^+$, even though the limited experimental data suggest that the $1/T_2$ values for $^{85}\text{Rb}^+$ are quite close to those of $^{87}\text{Rb}^+$ (see Ref. 70). Furthermore, from the few experimental results on $^{85}\text{Rb}^+$ that we found in the literature, we did observe significant variability, with a reported $1/T_2$ value of 512 s^{-1} at 4 m in Ref. 71 and a $1/T_1$ value of 710 s^{-1} at infinite dilution⁷². While comparing values with such differences in salt concentration is not optimal, it may contribute to the difference between the simulations and the experimental data. On the modelling side, this difference may also arise from the KJPAW pseudopotential used for calculating the effective Sternheimer factor with Rb^+ and Cs^+ , for which no GIPAW pseudopotentials were available. Comparing the results with both pseudopotentials for aqueous LiCl and NaCl resulted in larger effective Sternheimer factors with KJPAW, by a factor of 1.8 and 1.5, respectively. This order of magnitude is comparable to the overestimation predicted for the quadrupolar NMR relaxation rates for $^{87}\text{Rb}^+$ and $^{133}\text{Cs}^+$. It is also possible that for these heavier ions, relativistic effects that were not taken into account in the present work might play a role in the electronic response close to the nucleus.

For the alkaline earth cations Mg^{2+} and Ca^{2+} in their aqueous chloride solutions, the simulation results also agree qualitatively with the experiments. For MgCl_2 , even though the relative error is relatively high, with the simulation results being higher than the experimental values, it does follow a similar trend with molality, keeping in the range investigated range of molality studied an overestimation by a factor of ≈ 2 . For CaCl_2 , the results align well around $c = 2.4\text{ m}$ but slightly overestimate (resp. underestimate) at lower (resp. higher) concentrations, with a relative error of around 40% at the lowest and highest molalities. Considering the simplicity of the force field and the challenge in the description of the solvation shell (and corresponding charge distribution) around multivalent ions, the overall agreement between the predicted and experimental relaxation rates is satisfactory.

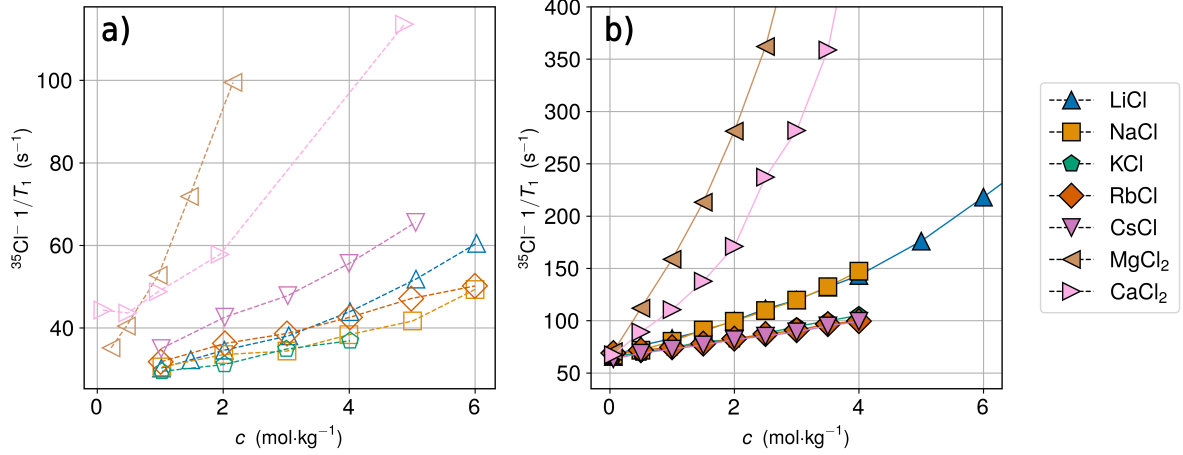


FIG. 4. NMR relaxation rates as a function of the molality for $^{35}\text{Cl}^-$, in aqueous LiCl, NaCl, KCl, RbCl, CsCl, MgCl_2 and CaCl_2 solutions. Open symbols represent the experimental data in (a), whereas full symbols correspond to the predictions of the present work from our simulations in (b). The values are compared to experimental values, with the following references: LiCl⁷³, NaCl⁷³, KCl⁷³, RbCl⁷³, CsCl⁷³, MgCl_2 ⁶⁸ and CaCl_2 ⁷⁴.

Finally, Figure 4 compares the predicted (full symbols) and experimental (open symbols) relaxation rates of the $^{35}\text{Cl}^-$ anion for all salts and molalities. As already observed for this anion at infinite dilution³³, the Madrid-2019 force field, together with the corresponding Sternheimer factor, leads to an overestimate of $1/T_1$. Nevertheless, the simulations reproduce qualitative trends with concentration observed experimentally. Specifically, the order of $1/T_1$ relaxation rates of Cl^- in the different systems is $\text{CsCl} < \text{RbCl} < \text{KCl} < \text{LiCl} < \text{NaCl} < \text{CaCl}_2 < \text{MgCl}_2$ for the simulation results, whereas the experimental order is $\text{KCl} < \text{RbCl} < \text{NaCl} < \text{LiCl} < \text{CsCl} < \text{CaCl}_2 < \text{MgCl}_2$. Thus, the most notable difference is the $1/T_1$ behaviour of $^{35}\text{Cl}^-$ in aqueous CsCl; in addition, the predictions overestimates the experimental rates by a factor $\approx 2 - 3$ in that case. For $^{35}\text{Cl}^-$ in aqueous LiCl (resp. NaCl), the overall factor is ≈ 2.8 (resp. 3.2), but is mainly due to the large overestimation (by ≈ 3.3 and 3.8 for LiCl and NaCl, respectively) for the largest molalities where both experimental and simulation data are available. For the other electrolytes, the overestimation factors depend slightly on concentration and are ≈ 2.7 for KCl, 2.3 for RbCl, 2.9 for MgCl_2 and 2.4 for CaCl_2 .

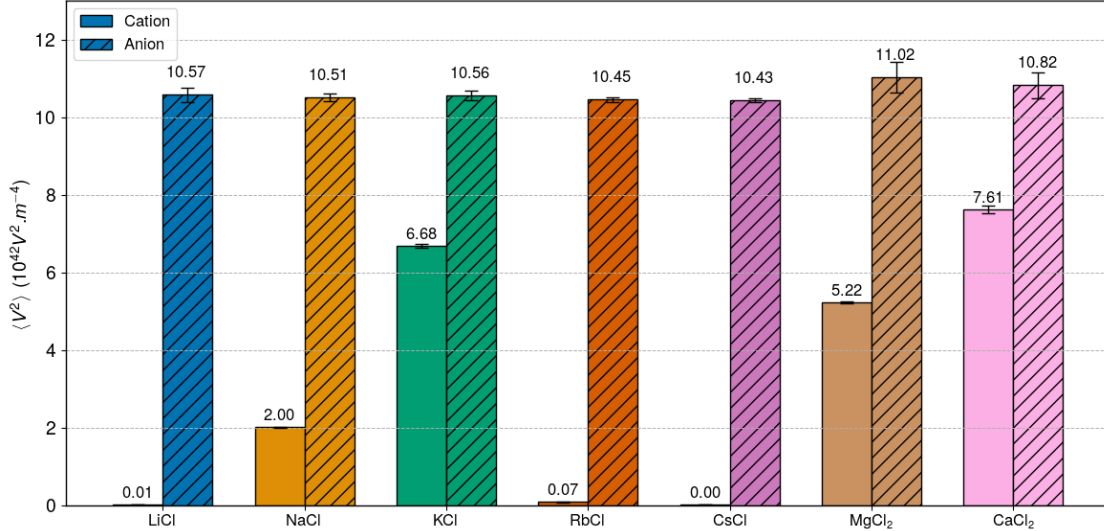


FIG. 5. EFG variance $\langle V^2 \rangle$ (including the effective Sternheimer factor) at the cation and anion positions for all the considered aqueous electrolytes. Results are shown averaged over all molalities, with errorbars indicating the associated standard deviations.

D. Static and dynamic effects on the quadrupolar NMR relaxation rate

We now investigate the role of static and dynamic effects reflected in changes in the total variance of the EFG, $\langle V^2 \rangle$, and the effective correlation time of the EFG, τ_c , at the cation and anion positions with varying salt concentrations. The results for the former, averaged over all concentrations, are presented in Fig. 5 (see SI Fig. S10 for the effect of concentration), while the latter are shown in Fig. 6. The EFG variance for cations only slightly depends on concentration, with a maximum change of $\approx 12\%$ between 0.06 m and 4 m in aqueous MgCl₂, all other systems displaying variations below 4%. In contrast, the EFG correlation time increases with concentration by factors that depend on the system. The largest increase is observed for LiCl, by a factor ≈ 11.9 from 0.06 m to 10 m, followed by MgCl₂, by a factor of ≈ 9.9 from 0.06 m to 4 m. For the other systems, this factor ranges from ≈ 1.4 to ≈ 1.6 .

Similarly, in the case of the anion, the total variance at the chlorine position does not change significantly with salt concentration, with the highest deviation observed in aqueous MgCl₂ at $\approx 12\%$ between 0.06 m and 4 m, followed by CaCl₂ with a deviation of $\approx 10\%$. For all other monovalent systems at the anion position, the deviation does not exceed 4%. In contrast, the EFG correlation time for the three aqueous systems LiCl, MgCl₂, and CaCl₂

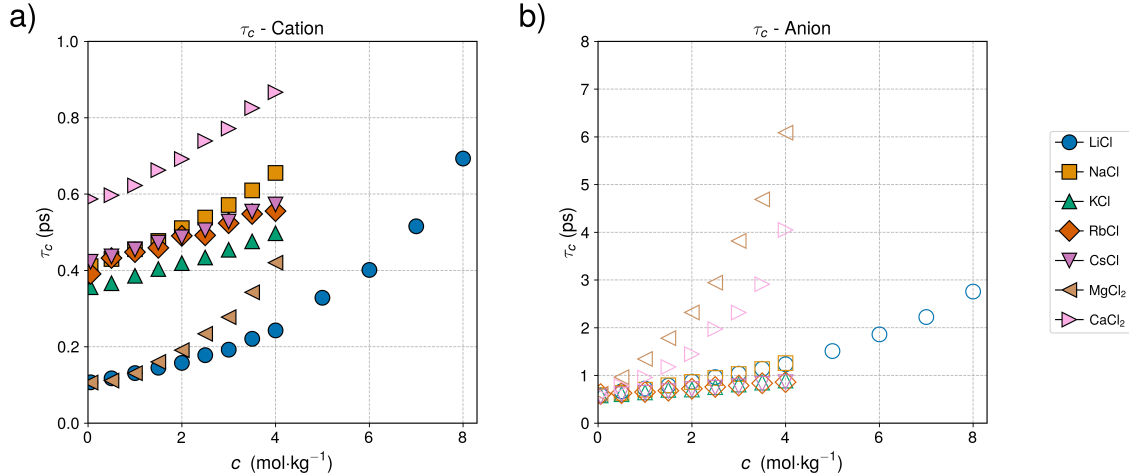


FIG. 6. Effective EFG correlation time τ_c for the cation (a) and anion (b) in aqueous LiCl, NaCl, KCl, RbCl, CsCl, MgCl₂ and CaCl₂ solutions, as a function of molality.

displays significant differences between the values at 0.06 m and at the highest molality, with factors of 7.6, 9.9, and 6.9, respectively. For all other systems, the EFG correlation time increases by a factor between 1.4 and 2.1. Overall, these observations indicate that the effect of concentration on the NMR relaxation rate for both cations and anions is primarily due to the changes in the EFG correlation time and that the effect of the changes in the variance only play a minor role. This generalizes the findings of Ref. 34 to the whole series of alkaline and alkaline earth chloride solutions considered in the present work.

For all cations and all concentrations considered, the EFG correlation time τ_c does not exceed 1 ps (see Fig. 6a). This is consistent with our results for NaCl with the same force field³⁴ as well as earlier studies in the literature for various cations through classical^{30,33,75,76} and ab initio MD simulations^{65,77,78}. Specifically, τ_c increases from 0.11 ps at 0.06 m to 1.27 ps at 10 m for Li⁺, from 0.41 ps to 0.65 ps between 0.06 m and 4 m for Na⁺, from 0.36 ps to 0.50 ps for K⁺, from 0.39 ps to 0.56 ps for Rb⁺, from 0.42 ps to 0.57 ps for Cs⁺, from 0.10 ps to 0.42 ps for Mg²⁺, and from 0.59 ps to 0.87 ps for Ca²⁺.

From their EFG correlation time τ_c at infinite dilution, the cations can be broadly categorized into three groups: one for all the monovalent cations except Li⁺, a second group with Li⁺ and Mg²⁺, and a third with Ca²⁺ only. All cations in the first group have similar EFG decorrelation times. The second group, which corresponds to the cations with tighter hydration shells, exhibit a faster EFG decorrelation. In addition, the tetrahedral symmetry

of the first hydration shell of Li^+ results in different EFG fluctuations compared to other ions³¹. Finally, the longest decorrelation is observed for Ca^{2+} , which has a less structured hydration shells. We note that the increase in τ_c with salt concentration between 0 and 4 m is more pronounced for the divalent cations, which might be related to the formation/breaking of ion pairs.

Despite these short correlation times, as mentioned above the integral defining τ_c (see Eq. 6) only converges over times larger by one to two orders of magnitude (see SI Fig. S9). Importantly, for all ions the integral of the slow, concentration-dependent decay of the EFG-ACF represents the main contribution ($\approx 90\%$) to τ_c , and hence to $1/T_1$, as observed for NaCl and shown for all ions in Fig. S7. This highlights the role of collective dynamics in the quadrupolar NMR relaxation of the ions, already essential at infinite dilution^{15,31}, and it is slowing down as the concentration increases³⁴. For the Cl^- anion in all the considered aqueous salts (see Fig. 6b), one also generally finds that $\tau_c \lesssim 1$ ps, except for the divalent salts MgCl_2 and CaCl_2 , as well as for LiCl beyond approximately 4 m. As for cations, τ_c increases with salt concentration and the integral of the slow, concentration-dependent decay of the EFG-ACF represents the main contribution ($\approx 90\%$) to τ_c , hence to $1/T_1$ (see SI Fig. S8).

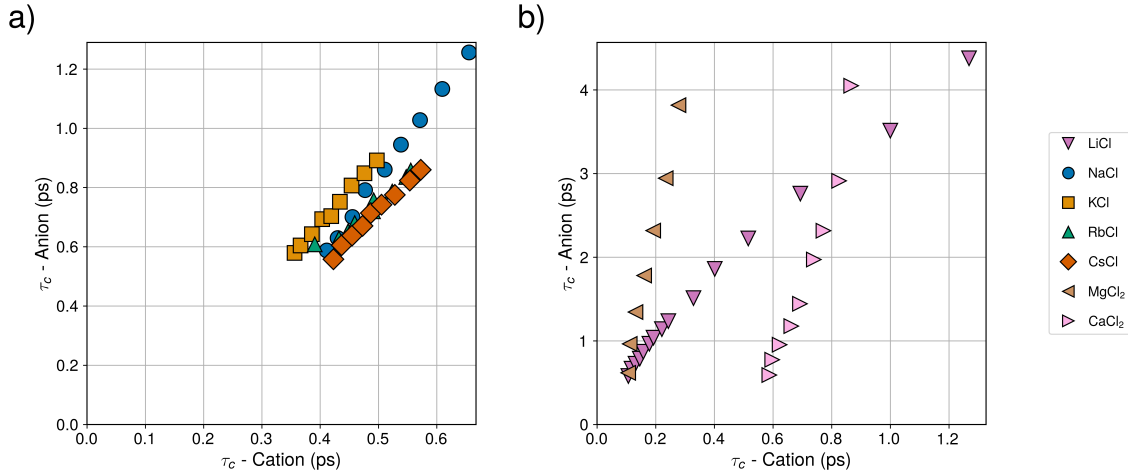


FIG. 7. Correlation between the EFG correlation times τ_c for the cation and anion in a) aqueous NaCl, KCl, RbCl, CsCl, and b) aqueous LiCl, MgCl_2 and CaCl_2 solutions.

It is instructive to compare the EFG correlation times for the cation and anion in each system. As illustrated in Fig. 7a, τ_c for the cations are similar for NaCl, KCl, RbCl and

CsCl, and so are τ_c for the anions in the same systems. Furthermore, the values for cations and anions are strongly correlated, with an approximately linear correlation, for this four systems the correlation time for anions being approximately 50% larger than for cations. In contrast (see Fig. 7b), for LiCl, MgCl₂ and CaCl₂, even though τ_c increases for both cations and anions when increasing the salt concentration, the respective times differ markedly – by a roughly constant factor ≈ 3.5 to 5 for LiCl, but varying from ≈ 6 to 14 for MgCl₂ and ≈ 1 to 5 for CaCl₂, depending on concentration.

Summarizing, in all systems the effect of concentration on the quadrupolar NMR relaxation rates of both cations and anions is primarily due to changes in the EFG decorrelation dynamics. Moreover, the slow decay of the EFG ACF (compared to the fast initial decay) provides the largest contribution to the overall relaxation and is well described by a stretched exponential, suggesting a broad distribution of relaxation modes arising from the coupling between the ions and the solvent dynamics. For the cations with a larger charge density (Li⁺ with a small radius and the divalent Mg²⁺ and Ca²⁺), the presence of ion pairs with the Cl⁻ may also play a role in the slowing down of the EFG fluctuations as the salt concentration increases.

E. Viscosity and diffusion coefficients

In order to correlate the above observations on the dynamics of the EFG fluctuations to the dynamics of the fluid, and before turning to the assessment of relaxation models in Section III F, we first discuss the predictions of the force field for the viscosity and diffusion coefficient of ions for all electrolytes over the considered concentration range. Fig. 8 shows that the viscosity at 25°C computed for all aqueous electrolytes from the stress ACF (discussed in Section III F below) in MD simulations via Eq. 7 is overall in good agreement with experimental data from the literature, particularly at low molality. At 0.06 m, the relative error w.r.t. the experiments is below 6% for all systems except LiCl ($\approx 19\%$). The agreement deteriorates for increasing concentration, with an average overestimation factor of 1.34 ± 0.08 across all systems at 4 m. This discrepancy becomes more pronounced at high molalities, as illustrated by the aqueous LiCl system, where an overestimation factor of 2.4 is observed at 10 m. Additionally, the experimental viscosity of RbCl and CsCl solutions exhibited a weak minimum at low molality. This subtle behaviour, as reported in Ref. 41, is

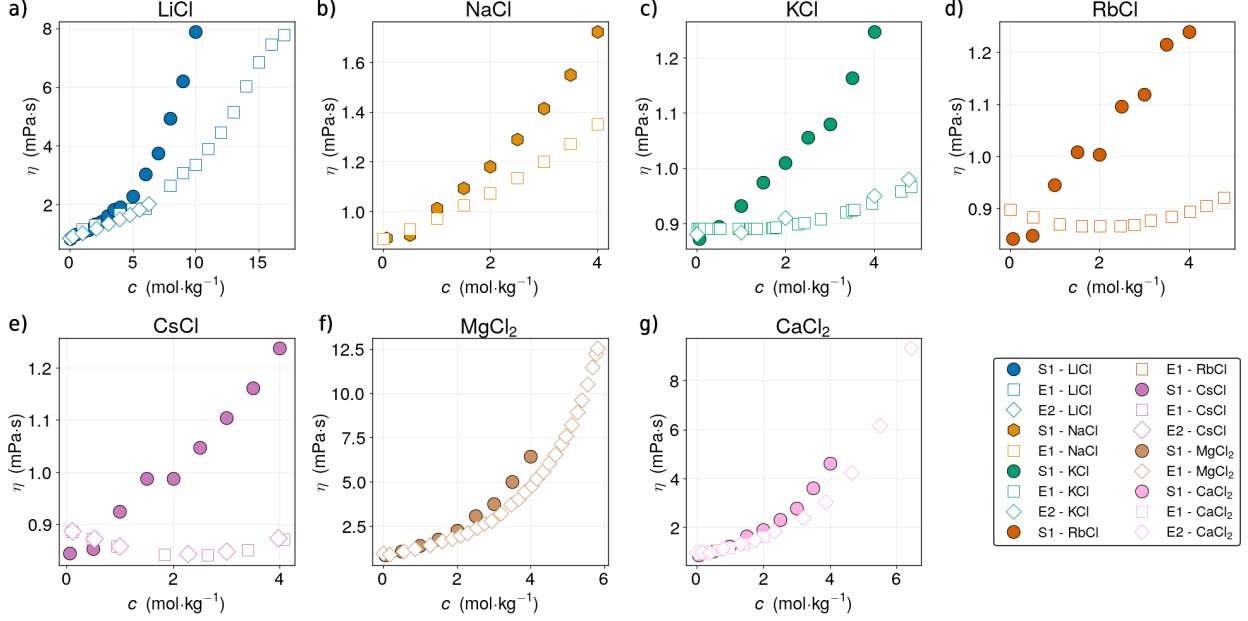


FIG. 8. Viscosity of aqueous (a) LiCl, (b) NaCl, (c) KCl, (d) RbCl, (e) CsCl, (f) MgCl₂, and (g) CaCl₂ solutions, as a function of molality. The simulation results obtained in this work (full symbols) are compared with experimental ones (open symbols) from the literature: LiCl from 32,79,80, NaCl from 81, KCl from 79,80,82, from RbCl 79,80, CsCl from 83, MgCl₂ from 79,80 and CaCl₂ from 79,80,84.

not captured by the the Madrid-2019 force field, which overestimates the viscosity for most of the concentration range for these salts.

In previous work³⁴, we have shown that the linear relation between the relaxation rate $1/T_1$ and the ratio between viscosity and thermal energy, $\eta/k_B T$, long known *e.g.* for polymers or colloids, and captured by the Stokes-Einstein-Debye model, also holds for the quadrupolar relaxation of Na⁺ cations in aqueous NaCl solutions, despite the limitations of the SED model in that case. Figs. 9 and 10 report $1/T_1$ as a function of $\eta/k_B T$ for cations and anions, respectively, for all considered aqueous solutions. The simulation results obtained in this work (full symbols) are compared with experimental ones (open symbols) from the literature.

Focusing first on cations (Fig. 9), for all systems except aqueous KCl, we observe a strong correlation between $1/T_1$ and $\eta/k_B T$ for both simulations and experimental results (linear regressions lead to $R^2 \geq 0.9$, with a minimum for CaCl₂). Consistently with the results of Figs. 3 and 8, the agreement between simulations and experiments is excellent for aqueous

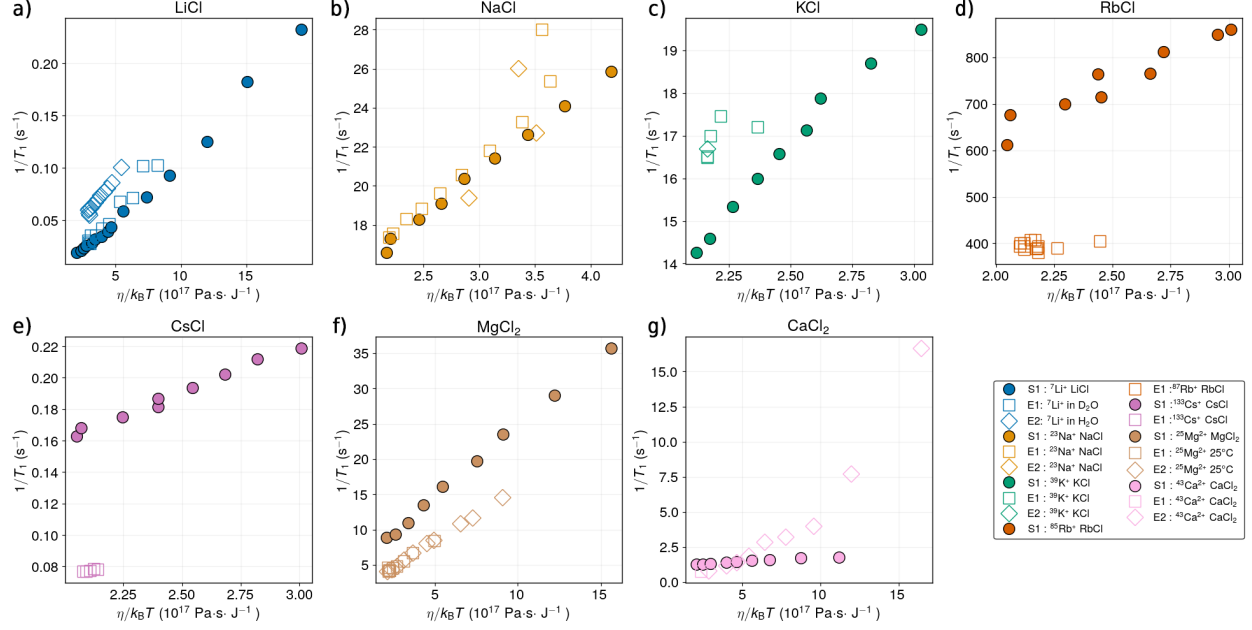


FIG. 9. Cation NMR relaxation rates $1/T_1$ in aqueous (a) LiCl, (b) NaCl, (c) KCl, (d) RbCl, (e) CsCl, (f) MgCl_2 , and (g) CaCl_2 solutions, as a function of the ratio between viscosity and thermal energy, $\eta/k_B T$. The simulation results obtained in this work (full symbols) are compared with experimental ones (open symbols) from the literature.

LiCl and NaCl, resulting in similar slopes for the correlations between $1/T_1$ and $\eta/k_B T$: 0.01245 (resp. 4.470) for the simulations, S1, and 0.01483 (resp. 6.172) for the experiment, E1, for LiCl (resp. NaCl). Relatively good agreement is also observed for aqueous CsCl (with slopes of 0.05888, S1, and 0.02419, E1) and MgCl_2 (with slopes of 2.016, S1, and 1.527, E1).

This is however not the case for RbCl (with slopes of 228.2, S1, and 15.99, E1) and CaCl_2 (with slopes of 0.06078, S1, and 1.100, E1), where the correlation between $1/T_1$ and $\eta/k_B T$ only separately holds for the simulations and experimental results. Several reasons might explain such discrepancy. In the RbCl case, it may derive from using the KJPAW pseudopotential to compute the effective Sternheimer factor and from the overestimation of the viscosity with the employed classical force field. For CaCl_2 , while the simulation and experimental values of $1/T_1$ and $\eta/k_B T$ are similar, their trends with concentration are quite different. As discussed above (see Figs. 3 and 8), this is mainly due to the effect of concentration on $1/T_1$, which is less well predicted than on the viscosity. Finally, for KCl the simulation and experimental results are similar, even though the experiments are not

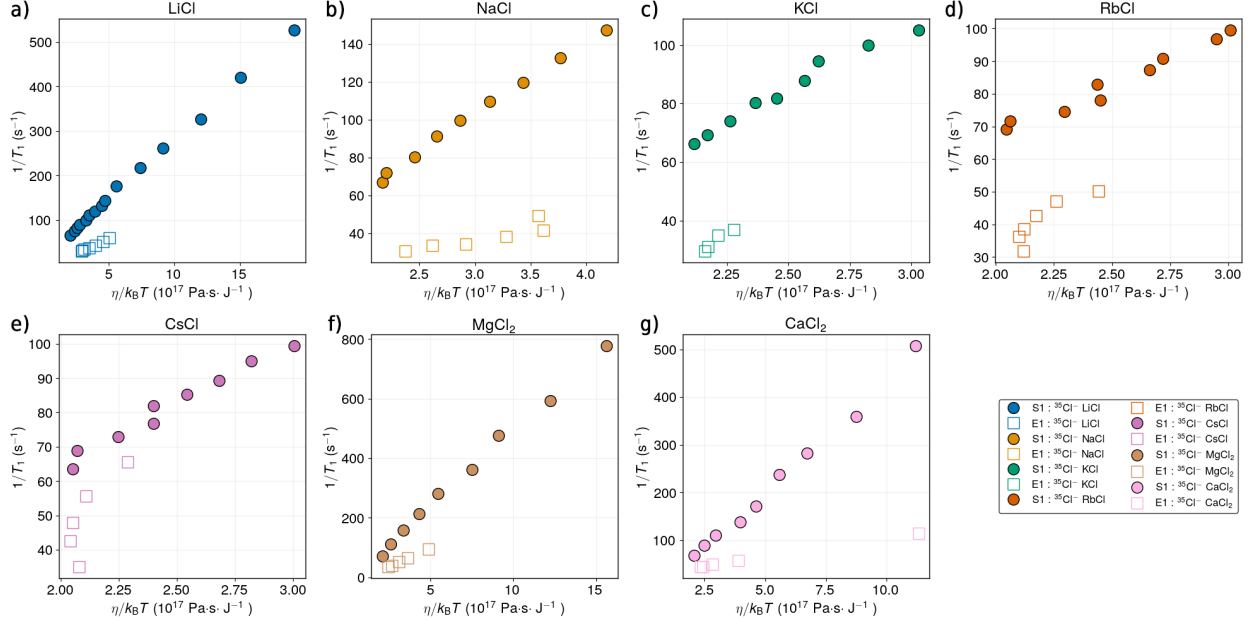


FIG. 10. Anion NMR relaxation rates $1/T_1$ in aqueous (a) LiCl, (b) NaCl, (c) KCl, (d) RbCl, (e) CsCl, (f) MgCl₂, and (g) CaCl₂ solutions, as a function of the ratio between viscosity and thermal energy, $\eta/k_B T$. The simulation results obtained in this work (full symbols) are compared with experimental ones (open symbols) from the literature.

well described by a linear fit.

For anions (see Fig. 10), we also observe a strong correlation between $1/T_1$ of $^{35}\text{Cl}^-$ and $\eta/k_B T$ for both simulations and experimental results. Linear regressions lead to $R^2 \geq 0.66$, with a minimum for CsCl, whose experimental trend of the viscosity with concentration is quite subtle, as discussed above, and all other values except for RbCl above 0.9. Overall, the correlation between $1/T_1$ and $\eta/k_B T$ for all ions suggests that ion mobility, shaped by interactions with the solvent, plays a crucial role in both the NMR relaxation rates and the viscosity of these systems. This will be further investigated in Section III F.

Since the Stokes-Einstein-Debye prediction of the relaxation rate (see Eqs. 11 and 12) involves the diffusion coefficient of the ion, we compare in Fig. 11 the cation diffusion coefficient at 25°C computed for all aqueous electrolytes with experimental data from the literature. While not always quantitative, especially for large salt concentrations, the simulation results are overall consistent with the experimental ones (as well as with previous simulation results with the same force field⁹², not shown). In all cases, cation diffusion coefficients decrease with increasing concentration, and water diffuses faster than both ions. For

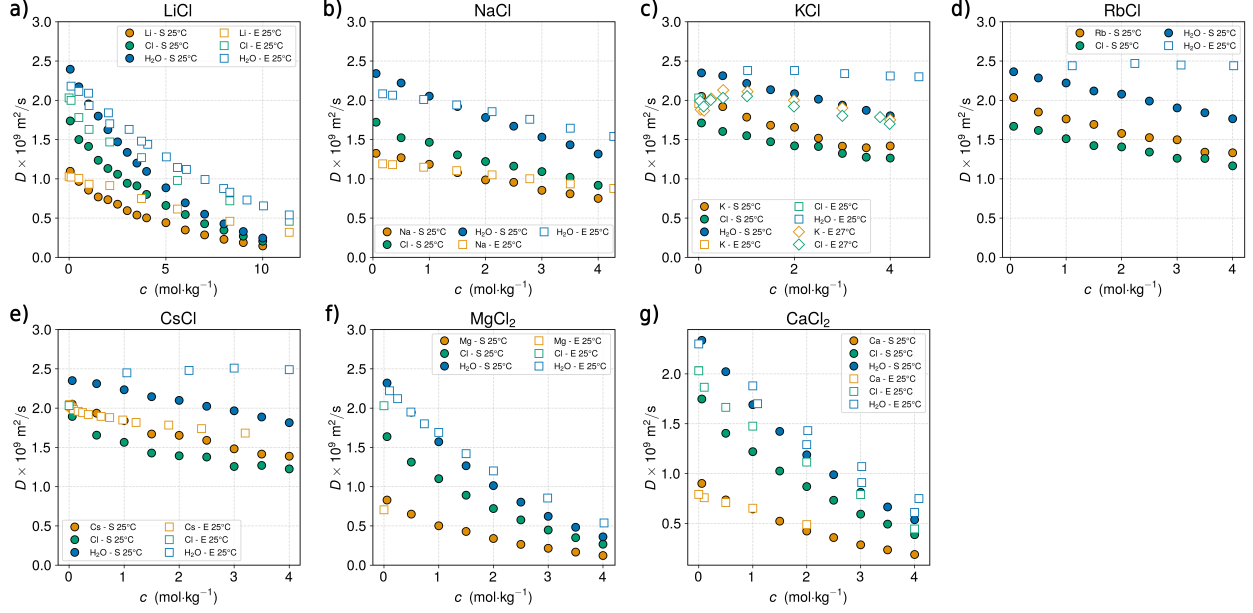


FIG. 11. Cation (orange), anion (green) and water (blue) diffusion coefficients in aqueous (a) LiCl, (b) NaCl, (c) KCl, (d) RbCl, (e) CsCl, (f) MgCl₂, and (g) CaCl₂ solutions, as a function of molality. The simulation results (S, full symbols) are compared to experimental data (E, open symbols) from the following references: for LiCl^{85–87}, KCl^{87,88}, CaCl₂^{87,89}, MgCl₂⁸⁷, CsCl^{87,90,91}, RbCl⁸⁷.

LiCl, NaCl, MgCl₂ and CaCl₂, the anion diffuses faster than the cation, while the opposite trend is observed for KCl, RbCl and CsCl. At the lowest molalities, the relative error with respect to experiments typically ranges between $\approx 5\text{-}12\%$; it increases to $\approx 20\%$ around 4 m and reaches $\approx 50\text{-}60\%$ in the aqueous LiCl system at 10 m. This aligns with the conclusion drawn from the viscosity that an increase in salt concentration leads to a deterioration of the predictive power of the force field for dynamical properties. Nevertheless, the agreement with experiments remains acceptable even at a few molals.

F. Assessment of relaxation models

Building upon the experimental and molecular simulation results presented in the previous sections, we now investigate the microscopic mechanisms underlying the NMR quadrupolar relaxation of the different cations and anions in the considered aqueous solutions.

1. Stokes-Einstein-Debye model

We first consider the Stokes-Einstein-Debye (SED) model of the EFG correlation time, τ_c^{SED} , given by Eq. 11, which corresponds to the EFG relaxation at the ion position is driven by Brownian rotational diffusion, likely linked to the collective reorientations of ion-water solvation complexes. Although the assumptions of the SED model are not expected to hold at the molecular scale⁹³⁻⁹⁷, we systematically explore τ_c^{SED} in relation to τ_c of the different cations across the seven systems, as it is commonly used to rationalize quadrupolar relaxation dynamics in liquids.

In practice, we estimate the hydrodynamic radii r_0 entering in Eq. 11 for the various cations using the concentration-dependent diffusion coefficients and viscosities obtained from our simulations (see Eq. 12). This is illustrated in Fig. S11 in the SI, which shows that D is indeed proportional to $k_B T / \eta$ and provides the corresponding r_0 . The simulated values for Li^+ , Na^+ , Rb^+ , and Cs^+ (2.31, 1.83, 1.34 and 1.31 Å, respectively) follow the same trend as the experimental one reported in Ref. 98 (3.37, 2.44, 1.90 and 1.70 Å, respectively), *i.e.* an overestimation by a factor ≈ 1.4 . K^+ has a hydrodynamic radius (1.31 Å) similar to Rb^+ and Cs^+ , while Mg^{2+} and Ca^{2+} possess the largest hydrodynamic radii: 3.01 Å and 2.78 Å, respectively. The hydrodynamic radius decreases increasing ionic radius (from 0.7 Å for Li^+ to 1.73 Å for Cs^+ , and from 0.7 Å for Mg^{2+} to 1.03 Å for Ca^{2+} , see Ref. 99) and increasing ionic charge. These trends are consistent with the previous study of Hayamizu *et al.*⁹⁸, and reflects the tighter hydration structure of ions when the electric field due to the ion is larger in the first hydration shell.

As shown in Fig. S12 in the SI, the resulting τ_c^{SED} indeed correlate with the simulation results τ_c for all cations. However, the SED model consistently overestimates the relaxation time, by a factor ranging from ~ 6 (for Rb^+ and Cs^+) to more than 100 for the divalent cations. Since Figs. 9 and 10 indicate a correlation between the relaxation rate and the ratio $\eta/k_B T$, as in the SED model, we extract an effective Stokes radius r_{eff} from the correlation between τ_c and $\eta/k_B T$, shown in Fig. S13, using a fit of the form:

$$\tau_c = \frac{4\pi\eta(r_{\text{eff}})^3}{3k_B T} + \tau_{\text{eff}}, \quad (14)$$

with an offset τ_{eff} (absent in the standard SED model) to improve the quality of the fit. The resulting r_{eff} are significantly smaller than the expected ionic radii, with values ranging from 0.38 Å for Mg^{2+} to 0.72 Å for K^+ and Cs^+ . Furthermore, for some cations, the inclusion of

an additional intercept τ_{eff} is necessary to accurately fit the data, as highlighted by Turton and Wynne⁹⁵, indicating the limitations of the SED model. Overall, these observations generalize to all considered electrolytes the ones made for aqueous NaCl in Ref. 34, and confirm that the SED model using the hydrodynamic radius corresponding to translational diffusion cannot predict the quadrupolar relaxation time.

2. Link between EFG and stress fluctuations

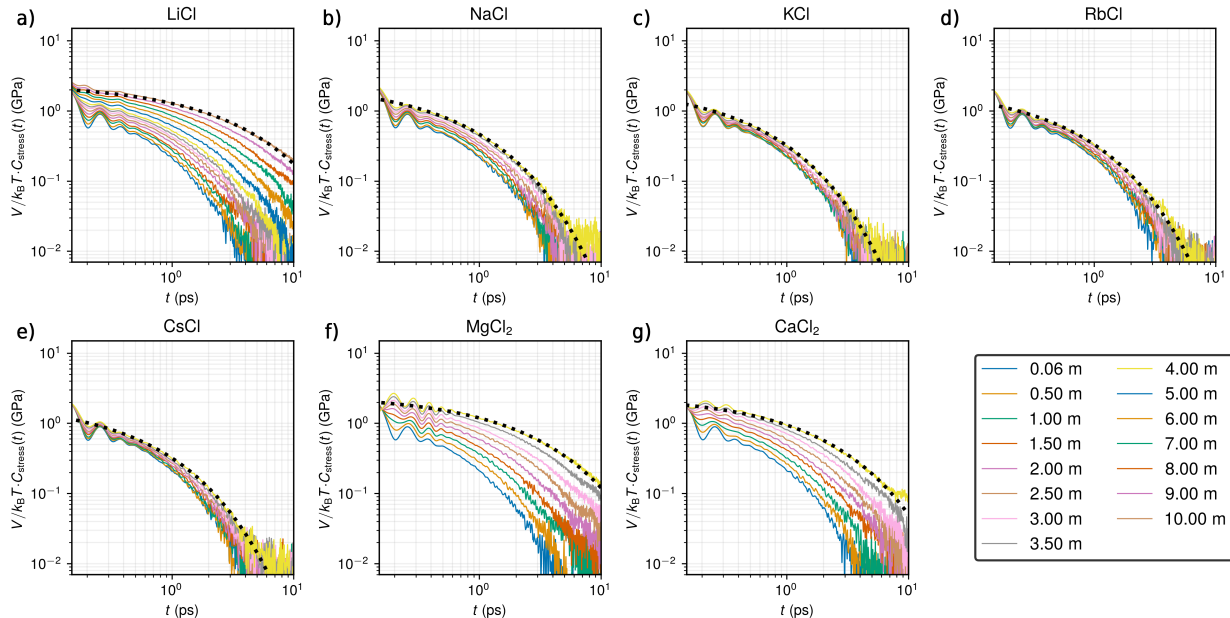


FIG. 12. Stress autocorrelation function (see Eq. 8) of aqueous (a) LiCl, (b) NaCl, (c) KCl, (d) RbCl, (e) CsCl, (f) MgCl₂, and (g) CaCl₂ solutions, as a function of molality (indicated by the color). Results are shown multiplied by $V/k_B T$, so that their integral from 0 to ∞ provides the viscosity (see Eq. 7). In each panel, the dotted black line corresponds to a fit to a stretched exponential of the decay at long time for the highest molality.

For aqueous NaCl, we recently found a good correlation between the EFG relaxation time for Na⁺ and the relaxation time of the stress tensor³⁴. As the EFG, the stress is a rank-2 tensor, and the integral of its ACF is related to the viscosity (see Eqs. 7 and 8), just as that of the EFG is related to the quadrupolar NMR relaxation rate. Here we find that for all the considered electrolytes the stress ACF exhibits a long-time tail, whose decay is slowed down with increasing salt concentration, indicating an overall deceleration of the viscous

dynamics of the liquid (see Fig. 12). A characteristic timescale can be defined as usual as the integral of the normalized ACF. Since the long-time tail of $C_{\text{stress}}(t)$ is well-described beyond a few tens of femtoseconds by a stretched exponential decay, ($\sim e^{-(t/\tau_k)^{\beta_k}}$, shown as dashed lines in Fig. 12), we obtain with this form the mean structural relaxation time $\tau_{\text{struct}} = \tau_k \beta_k^{-1} \Gamma(\beta_k^{-1})$. Following Ref. 34, for all systems we used $\beta_k = 0.61$ and considered only τ_k as a fitting parameter, with values around 0.25 ps for all systems at 0.06 m, an increase with concentration up to 0.4 ps (resp. more than 1 ps) for monovalent (resp. divalent) ions at 4 m, and a further to 2.05 ps at 10 m for aqueous LiCl.

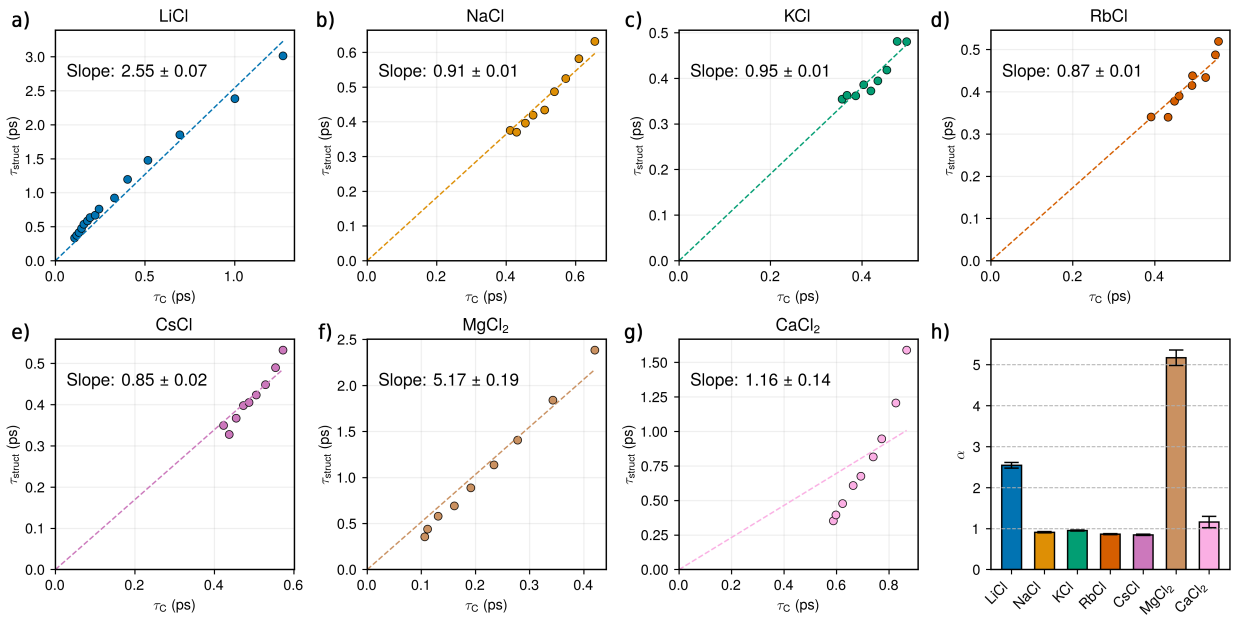


FIG. 13. Comparison between the structural relaxation time τ_{struct} and the EFG correlation time τ_c of cations in aqueous (a) LiCl, (b) NaCl, (c) KCl, (d) RbCl, (e) CsCl, (f) MgCl_2 , and (g) CaCl_2 solutions. The dashed lines represent linear fits defined as $\tau_{\text{struct}} = a \tau_c$ with the cation-specific slopes a indicated in each panel and summarized in the last panel as a bar plot. The data for CaCl_2 is not well described by such a fit, but we provide the corresponding slope for completeness.

The resulting structural relaxation time τ_{struct} , shown for all salts as a function of concentration in Fig. S14, is compared with the EFG relaxation time of cations, for all considered electrolytes in Fig. 13. As in the case of NaCl in Ref. 34, we find in all cases except CaCl_2 that they are approximately proportional to each other, *i.e.* $\tau_{\text{struct}} \approx a \tau_c$. In addition, the proportionality factor a is close to one (0.91, 0.95, 0.87 and 0.85 for Na^+ , K^+ , Rb^+ and Cs^+ , respectively) for all monovalent cations except Li^+ ($a \approx 2.55$). Even though the stress

and EFG tensors are not directly related, both quantities are inherently collective and the decay of their ACFs is primarily governed by many-body correlations and exhibits a similar stretched decay for $t > 0.4 - 0.5$ ps. These observations suggest that, in all these systems, the fast collective dynamics of the liquid, which drive their structural rearrangements, play a key role in quadrupolar NMR relaxation.

For MgCl_2 , the linear relation still holds, but as for LiCl the proportionality factor significantly deviates from 1 ($a = 5.17$). In both cases, this might be attributed to the tighter solvation shells of these ions, already mentioned when discussing the viscosity or the hydrodynamic radius, which may result in a weaker coupling with water molecules further from the ions. One can hypothesize that the collective relaxation in that case can be represented as arising from the coupling between the dynamics of (large) hydrated ions in the remaining solvent (similar to Na^+ , K^+ , Rb^+ and Cs^+), the internal dynamics of this species (within the hydration shell) and the exchange of solvent molecules in and out of the hydration shell. For aqueous CaCl_2 , while there is a clear correlation between the structural relaxation times, a fit by $\tau_{\text{struct}} \approx a \tau_c$ is clearly not a good representation of the data, suggesting a more complex interplay between the system's structural relaxation and the EFG relaxation of the cation.

In the specific case of LiCl , an additional deviation from the linear regime described by $\tau_{\text{struct}} = a \tau_c$ occurs at molalities higher than 4 m, requiring an additional intercept to accurately fit the values of the two relaxation times. This deviation could arise from different sources, including i) limitations of the force field used: Deviations from experimental results are also observed at higher molalities, suggesting the force field might not fully capture the system's behaviour; ii) structural deformation: From our previous study concerning Na^+ , τ_c appears to primarily depend on the first two hydration shells. At increasing molalities, overlapping of hydration shells is likely to occur. This could form specific hydration structures around lithium, significantly affecting τ_c . The second explanation could align with previous studies^{100,101} suggesting that the increased molality distorts the hydration shell of Li^+ ions and change its hydration number.

IV. CONCLUSION

We investigated the quadrupolar NMR relaxation of cations and anions in aqueous electrolyte solutions, including NaCl , LiCl , KCl , RbCl , CsCl , MgCl_2 , and CaCl_2 , across a broad

range of salt concentrations, using molecular simulations. To that end, we used our previously introduced approach combining DFT-PAW calculations and classical molecular dynamics to compute the electric field gradient fluctuations over the relevant time scales. The predicted NMR relaxation rates $1/T_1$ are in good agreement with experiments from the literature, quantitative up to a few molals for some cations, and qualitative (even though overestimated) for the $^{35}\text{Cl}^-$ anion across the 7 aqueous solutions.

We analyzed the contributions of static and dynamic effects to the quadrupolar NMR relaxation rates. Our results demonstrate that the growth of $1/T_1$ for the various ions with increasing salt concentration is primarily driven by a slowing down of the EFG fluctuations, and that the variance of the EFG at the ion positions does not vary significantly with concentration. For all ions, the main contribution to the EFG correlation time τ_c arises from the second, slower decay mode of the EFG ACF, which could be fitted with a stretched exponential, suggesting a broad distribution of relaxation modes. We highlighted the different behaviour of smaller (Li^+) and divalent (Mg^{2+} and Ca^{2+}), compared to the other monovalent cations, which points to the effect of their tighter solvation shells and of the possible role of ion pair formation in the decay of the EFG fluctuations.

For low molalities, the experimental viscosity of all aqueous solutions is generally well reproduced by the classical force field used, although some specific behaviours, previously highlighted in Refs. 40 and 41 are not accurately captured. The linear correlation between $1/T_1$ and the viscosity ($\eta/k_B T$), which usually motivates the use of the Stokes-Einstein-Debye model, approximately holds in these systems both in simulations and experiments. By estimating the SED relaxation time from the concentration-dependent viscosities and ion diffusion coefficients in our simulations. Even though the hydrodynamic radii deduced from the diffusion coefficients are reasonable and the SED relaxation time correlates with τ_c , it is systematically larger (by at least a factor of 6-7), as observed for Na^+ in aqueous NaCl solution in Ref. 34.

In contrast, the structural relaxation time scale extracted from the fluctuations of the stress tensor introduced in the same reference is proportional to τ_c (except for aqueous CaCl_2), and within 15% of its value for all monovalent salts except LiCl . Even though the stress and EFG tensors are not directly related, both quantities are inherently collective, *i.e.* the relaxation of their fluctuations is primarily governed by many-body correlations. Thus, the fast collective dynamics of the liquid, which drive their structural arrangements,

also play a key role in quadrupolar NMR relaxation. Similar conclusions can be drawn for LiCl and MgCl₂, even though their tighter solvation shells result in a faster decorrelation of the EFG fluctuations compared to that of the stress tensor. These results generalize in particular the observation for Na⁺ in aqueous NaCl solution that models assuming a viscous model of the solvent dynamics, such as the SED, are not sufficient to describe the EFG fluctuations, since they assume a fast decay of the stress fluctuations compared to that of the EFG.

The detailed microscopic mechanisms leading to the above-mentioned structural rearrangements and their effects on both the stress and EFG relaxation remain however to be clarified, and it might be particularly useful to combine the information on the NMR relaxation of ions with that of water¹⁰² or insights from other experimental techniques. It would in particular be interesting to consider the role of discrete events whereby water molecules change of partner within the hydrogen bond network, described by the so-called "jump model"^{93,94,96,97,103}. In addition to considering more complex systems such as water-in-salt electrolytes, which contain more ions than water, it is also relevant to develop analytical theories accounting for the effect of salt concentration on the EFG relaxation, building on implicit solvent descriptions of electrolytes such as the ones developed to predict the electrical conductivity¹⁰⁴.

ACKNOWLEDGMENTS

We thank Alexej Jerschow, Guillaume Mériduet and Anne-Laure Rollet for useful discussions. This project received funding from the European Research Council under the European Union's Horizon 2020 research and innovation program (grant agreement no. 863473). This work was performed using HPC resources from GENCI-IDRIS (Grant-2024-AD010912966R2).

AUTHOR DECLARATIONS

Conflict of interest

There is no conflict of interest to declare

Author contributions

Matthieu Wolf: Conceptualization (equal); Formal analysis (equal); Investigation (lead); Methodology (supporting); Software (supporting); Writing/Original Draft Preparation (lead); Writing – review & editing (equal). **Iurii Chubak:** Conceptualization (equal); Formal analysis (equal); Investigation (supporting); Methodology (supporting); Software (lead); Writing – review & editing (equal). **Benjamin Rotenberg:** Conceptualization (lead); Formal analysis (equal); Funding Acquisition (lead); Investigation (supporting); Methodology (lead); Supervision (lead); Writing – review & editing (equal).

DATA AVAILABILITY

To be completed consistently with the final version of the manuscript: The original data presented in this study are openly available in Zenodo at [DOI/URL] or [reference/accession number].

REFERENCES

- ¹H. Ohtaki and T. Radnai, *Chem. Rev.*, 1993, **93**, 1157–1204.
- ²G. Madelin, J.-S. Lee, R. R. Regatte and A. Jerschow, *Prog. Nucl. Magn. Reson. Spectrosc.*, 2014, **79**, 14–47.
- ³G. Madelin, *X-Nuclei Magnetic Resonance Imaging*, CRC Press, 2022.
- ⁴S. Chandrashekar, N. M. Trease, H. J. Chang, L.-S. Du, C. P. Grey and A. Jerschow, *Nature Mater.*, 2012, **11**, 311–315.
- ⁵O. Pecher, J. Carretero-González, K. J. Griffith and C. P. Grey, *Chem. Mater.*, 2017, **29**, 213–242.
- ⁶A. Abragam, *The Principles of Nuclear Magnetism*, Oxford university press, 1961.
- ⁷J. E. Roberts and J. Schnitker, *J. Phys. Chem.*, 1993, **97**, 5410–5417.
- ⁸J. T. Hynes and P. G. Wolynes, *J. Chem. Phys.*, 1981, **75**, 395–401.
- ⁹B.-C. Perng and B. M. Ladanyi, *J. Chem. Phys.*, 1998, **109**, 676–684.
- ¹⁰J. Bosse, D. Quitmann and C. Wetzel, *Phys. Rev. A*, 1983, **28**, 2459–2473.
- ¹¹H. G. Hertz, *Ber. Bunsenges. Phys. Chem.*, 1973, **77**, 531–540.
- ¹²H. G. Hertz, *Ber. Bunsenges. Phys. Chem.*, 1973, **77**, 688–697.

- ¹³H. G. Hertz, M. Holz, G. Keller, H. Versmold and C. Yoon, *Ber. Bunsenges. Phys. Chem.*, 1974, **78**, 493–509.
- ¹⁴H. Versmold, *Mol. Phys.*, 1986, **57**, 201–216.
- ¹⁵A. Carof, M. Salanne, T. Charpentier and B. Rotenberg, *J. Chem. Phys.*, 2016, **145**, 124508.
- ¹⁶W. S. Price, B. E. Chapman and P. W. Kuchel, *Bull. Chem. Soc. Jpn.*, 1990, **63**, 2961–2965.
- ¹⁷J. Mitchell, *J. Pet. Sci. Eng.*, 2016, **146**, 360–368.
- ¹⁸C. D’Agostino, S. J. Davis and A. P. Abbott, *J. Chem. Phys.*, 2021, **154**, 224501.
- ¹⁹M. Eisenstadt and H. L. Friedman, *J. Chem. Phys.*, 1966, **44**, 1407–1415.
- ²⁰M. Eisenstadt and H. L. Friedman, *J. Chem. Phys.*, 1967, **46**, 2182–2193.
- ²¹A. Abragam, *The Principles of Nuclear Magnetism*, Oxford University Press, 1961.
- ²²S. Badu, L. Truflandier and J. Autschbach, *J. Chem. Theory Comput.*, 2013, **9**, 4074–4086.
- ²³J. Schmidt, J. Hutter, H.-W. Spiess and D. Sebastiani, *ChemPhysChem*, 2008, **9**, 2313–2316.
- ²⁴A. Philips, A. Marchenko, L. A. Truflandier and J. Autschbach, *J. Chem. Theory Comput.*, 2017, **13**, 4397–4409.
- ²⁵A. Philips, A. Marchenko, L. C. Ducati and J. Autschbach, *J. Chem. Theory Comput.*, 2019, **15**, 509–519.
- ²⁶A. Philips and J. Autschbach, *J. Chem. Theory Comput.*, 2020, **16**, 5835–5844.
- ²⁷S. Engström, B. Jönsson and B. Jönsson, *J. Magn. Reson. (1969-1992)*, 1982, **50**, 1–20.
- ²⁸S. Engström, B. Jönsson and R. W. Impey, *J. Chem. Phys.*, 1984, **80**, 5481–5486.
- ²⁹P. Linse and B. Halle, *Mol. Phys.*, 1989, **67**, 537–573.
- ³⁰A. Carof, M. Salanne, T. Charpentier and B. Rotenberg, *J. Phys. Chem. B*, 2014, **118**, 13252–13257.
- ³¹A. Carof, M. Salanne, T. Charpentier and B. Rotenberg, *J. Chem. Phys.*, 2015, **143**, 194504.
- ³²M. Mohammadi, S. Benders and A. Jerschow, *J. Chem. Phys.*, 2020, **153**, 184502.
- ³³I. Chubak, L. Scalfi, A. Carof and B. Rotenberg, *J. Chem. Theory Comput.*, 2021, **17**, 6006–6017.

- ³⁴I. Chubak, L. Alon, E. V. Silletta, G. Madelin, A. Jerschow and B. Rotenberg, *Nat. Commun.*, 2023, **14**, 1–10.
- ³⁵R. Sternheimer, *Phys. Rev.*, 1950, **80**, 102–103.
- ³⁶R. M. Sternheimer, *Phys. Rev.*, 1966, **146**, 140–160.
- ³⁷J. Autschbach, S. Zheng and R. W. Schurko, *Concepts Magn. Reson. A*, 2010, **36A**, 84–126.
- ³⁸P. E. Blöchl, *Phys. Rev. B*, 1994, **50**, 17953–17979.
- ³⁹T. Charpentier, *Solid State Nucl. Magn. Reson.*, 2011, **40**, 1–20.
- ⁴⁰I. M. Zeron, J. L. F. Abascal and C. Vega, *J. Chem. Phys.*, 2019, **151**, 134504.
- ⁴¹S. Blazquez, M. M. Conde, J. L. F. Abascal and C. Vega, *The Journal of Chemical Physics*, 2022, **156**, 044505.
- ⁴²J. L. F. Abascal and C. Vega, *J. Chem. Phys.*, 2005, **123**, 234505.
- ⁴³B. J. Kirby and P. Jungwirth, *The Journal of Physical Chemistry Letters*, 2019, **10**, 7531–7536.
- ⁴⁴A. Marin-Lafèche, M. Haeefe, L. Scalfi, A. Coretti, T. Dufils, G. Jeanmairet, S. K. Reed, A. Serva, R. Berthin, C. Bacon, S. Bonella, B. Rotenberg, P. A. Madden and M. Salanne, *J. Open Source Softw.*, 2020, **5**, 2373.
- ⁴⁵A. Coretti, C. Bacon, R. Berthin, A. Serva, L. Scalfi, I. Chubak, K. Goloviznina, M. Haeefe, A. Marin-Lafèche, B. Rotenberg, S. Bonella and M. Salanne, *J. Chem. Phys.*, 2022, **157**, 184801.
- ⁴⁶A. Aguado and P. A. Madden, *J. Chem. Phys.*, 2003, **119**, 7471–7483.
- ⁴⁷H. M. Foley, R. M. Sternheimer and D. Tycko, *Phys. Rev.*, 1954, **93**, 734–742.
- ⁴⁸N. Varini, D. Ceresoli, L. Martin-Samos, I. Girotto and C. Cavazzoni, *Comput. Phys. Commun.*, 2013, **184**, 1827–1833.
- ⁴⁹C. Tantardini, A. G. Kvashnin and D. Ceresoli, *Materials*, 2022, **15**, 3347.
- ⁵⁰A. Dal Corso, *Comput. Mater. Sci.*, 2014, **95**, 337–350.
- ⁵¹T. Chen, B. Smit and A. T. Bell, *J. Chem. Phys.*, 2009, **131**, 246101.
- ⁵²I.-C. Yeh and G. Hummer, *J. Phys. Chem. B*, 2004, **108**, 15873–15879.
- ⁵³P. Debye, *Polar Molecules*, Dover, 1929.
- ⁵⁴A. Einstein, *Investigations on the Theory of the Brownian Movement*, Dover, 1956.
- ⁵⁵J. Mähler and I. Persson, *Inorg. Chem.*, 2012, **51**, 425–438.
- ⁵⁶M. I. Bernal-Uruchurtu and I. Ortega-Blake, *J. Chem. Phys.*, 1995, **103**, 1588–1598.

- ⁵⁷A. Bhattacharjee, A. B. Pribil, B. R. Randolph, B. M. Rode and T. S. Hofer, *Chem. Phys. Lett.*, 2012, **536**, 39–44.
- ⁵⁸S. Friesen, G. Hefter and R. Buchner, *J. Phys. Chem. B*, 2019, **123**, 891–900.
- ⁵⁹D. E. Woessner, B. S. Snowden and A. G. Ostroff, *J. Chem. Phys.*, 1968, **49**, 371–375.
- ⁶⁰B. V. I. Chizhik, *Mol. Phys.*, 1997, 653–660.
- ⁶¹W. Sahn and A. Schwenk, *Zeitschrift für Naturforschung A*, 1974, **29**, 1754–1762.
- ⁶²K. FUMINO, A. SHIMIZU and Y. TANIGUCHI, *Denki Kagaku oyobi Kogyo Butsuri Kagaku*, 1997, **65**, 198–203.
- ⁶³H. Hertz, M. Holz and A. Sacco, *Chemica Scripta*, 1989, **29**, 21–2.
- ⁶⁴E. Detscher, H. G. Hertz, M. Holz and X.-a. Mao, *Zeitschrift für Naturforschung A*, 1995, **50**, 487–501.
- ⁶⁵A. Philips and J. Autschbach, *J. Chem. Theory Comput.*, 2020, **16**, 5835–5844.
- ⁶⁶K. Fumino, M. Kato and Y. Taniguchi, *J. Mol. Liq.*, 2002, **100**, 119–128.
- ⁶⁷T. Asakura and N. Nakayama, *Sen'i Gakkaishi*, 1989, **45**, 252–257.
- ⁶⁸R. Struis, J. De Bleijser and J. Leyte, *The Journal of Physical Chemistry*, 1989, **93**, 7932–7942.
- ⁶⁹M. Holz, S. Günther, O. Lutz, A. Nolle and P.-G. Schrade, *Zeitschrift für Naturforschung A*, 1979, **34**, 944–949.
- ⁷⁰B. Lindman and I. Danielsson, *J. Colloid Interface Sci.*, 1972, **39**, 349–356.
- ⁷¹C. Deverell and R. E. Richards, *Mol. Phys.*, 1966, **10**, 551–564.
- ⁷²D. E. O'Reilly and E. M. Peterson, *J. Chem. Phys.*, 1969, **51**, 4906–4908.
- ⁷³M. Holz and H. Weingärtner, *Journal of Magnetic Resonance (1969)*, 1977, **27**, 153–155.
- ⁷⁴P. Yu and R. J. Kirkpatrick, *Cem. Concr. Res.*, 2001, **31**, 1479–1485.
- ⁷⁵S. Engström, B. Jönsson and B. Jönsson, *Journal of Magnetic Resonance (1969)*, 1982, **50**, 1–20.
- ⁷⁶J. E. Roberts and J. Schnitker, *The Journal of Physical Chemistry*, 1993, **97**, 5410–5417.
- ⁷⁷S. Badu, L. Truflandier and J. Autschbach, *J. Chem. Theory Comput.*, 2013, **9**, 4074–4086.
- ⁷⁸A. Philips, A. Marchenko, L. A. Truflandier and J. Autschbach, *J. Chem. Theory Comput.*, 2017, **13**, 4397–4409.
- ⁷⁹M. Laliberté, *J. Chem. Eng. Data*, 2007, **52**, 321–335.
- ⁸⁰M. Laliberté, *J. Chem. Eng. Data*, 2009, **54**, 1725–1760.

- ⁸¹J. Kestin, H. E. Khalifa and R. J. Correia, *J. Phys. Chem. Ref. Data*, 1981, **10**, 71–88.
- ⁸²Zhang and Han, *J. Chem. Eng. Data*, 1996, **41**, 516–520.
- ⁸³T. Nakai, S. Sawamura and Y. Taniguchi, in *Studies in Physical and Theoretical Chemistry*, Elsevier, Waltham, MA, USA, 1995, vol. 83, pp. 365–368.
- ⁸⁴I. M. Abdulagatov and N. D. Azizov, *Fluid Phase Equilib.*, 2006, **240**, 204–219.
- ⁸⁵I. Pethes, *J. Mol. Liq.*, 2017, **242**, 845–858.
- ⁸⁶K. Tanaka and M. Nomura, *J. Chem. Soc., Faraday Trans. 1 F*, 1987, **83**, 1779–1782.
- ⁸⁷K. J. Müller and H. G. Hertz, *J. Phys. Chem.*, 1996, **100**, 1256–1265.
- ⁸⁸M. A. Esmailbeig and S. Movahedirad, *Korean J. Chem. Eng.*, 2017, **34**, 977–986.
- ⁸⁹H. G. Hertz and R. Mills, *J. Phys. Chem.*, 1978, **82**, 952–959.
- ⁹⁰H. Chakrabarti, *Appl. Radiat. Isot.*, 1994, **45**, 171–175.
- ⁹¹R. Mills and V. M. Lobo, *Self-diffusion in electrolyte solutions: a critical examination of data compiled from the literature*, Elsevier, 2013.
- ⁹²I. M. Zeron, J. L. F. Abascal and C. Vega, *J. Chem. Phys.*, 2019, **151**, 134504.
- ⁹³D. Laage and J. T. Hynes, *Science*, 2006, **311**, 832–835.
- ⁹⁴G. Stirnemann, E. Wernersson, P. Jungwirth and D. Laage, *Journal of the American Chemical Society*, 2013, **135**, 11824–11831.
- ⁹⁵D. A. Turton and K. Wynne, *J. Phys. Chem. B*, 2014, **118**, 4600–4604.
- ⁹⁶D. Laage and G. Stirnemann, *The Journal of Physical Chemistry B*, 2019, **123**, 3312–3324.
- ⁹⁷E. Pluhařová, G. Stirnemann and D. Laage, *Journal of Molecular Liquids*, 2022, **363**, 119886.
- ⁹⁸K. Hayamizu, Y. Chiba and T. Haishi, *RSC Adv.*, 2021, **11**, 20252–20257.
- ⁹⁹Y. Marcus, *Chem. Rev.*, 1988, **88**, 1475–1498.
- ¹⁰⁰I. Harsányi and L. Pusztai, *J. Chem. Phys.*, 2005, **122**, 124512.
- ¹⁰¹I. Harsányi, Ph. A. Bopp, A. Vrhovšek and L. Pusztai, *J. Mol. Liq.*, 2011, **158**, 61–67.
- ¹⁰²C. Zhang and A. Jerschow, *The Journal of Chemical Physics*, 2024, **160**, 154501.
- ¹⁰³A. Gomez, Z. A. Piskulich, W. H. Thompson and D. Laage, *The Journal of Physical Chemistry Letters*, 2022, **13**, 4660–4666.
- ¹⁰⁴P. Illien, A. Carof and B. Rotenberg, *Phys. Rev. Lett.*, 2024, **133**, 268002.

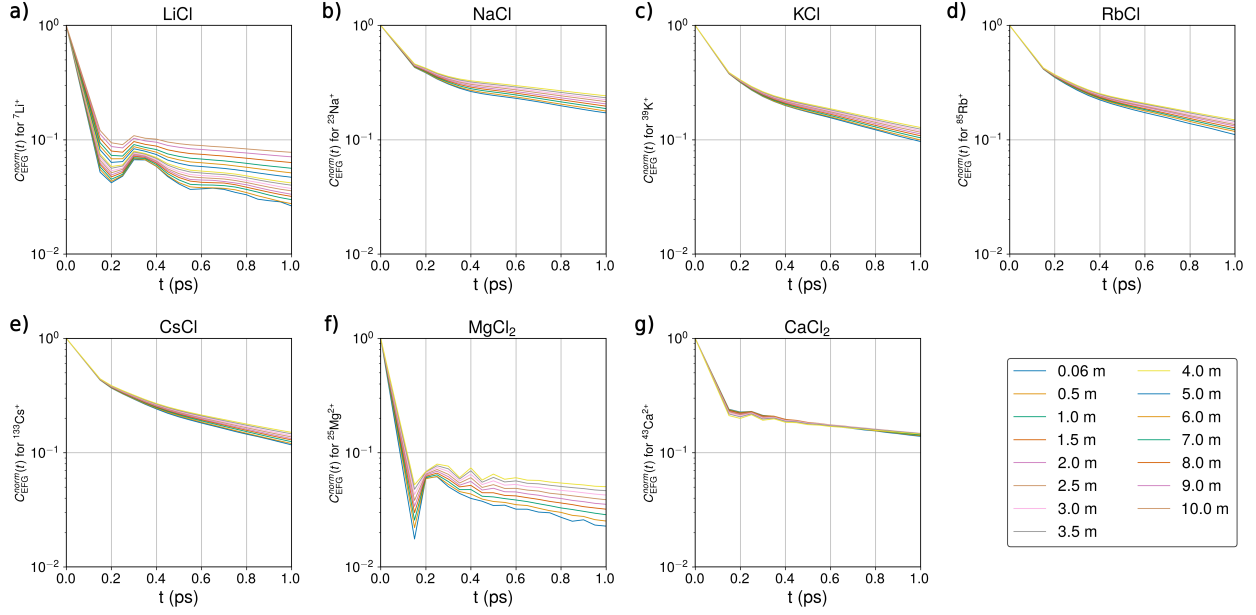


Fig. S1. Normalized autocorrelation function of the electric field gradient at the cation position in aqueous (a) LiCl, (b) NaCl, (c) KCl, (d) RbCl, (e) CsCl, (f) MgCl₂, and (g) CaCl₂ as a function of time from 0 to 1 ps, presented for various molalities.

System	β - Cation	β - Anion
LiCl	0.5202	0.6980
NaCl	0.6747	0.6793
KCl	0.5129	0.7572
RbCl	0.6025	0.6813
CsCl	0.5464	0.7486
MgCl ₂	0.4583	0.4475
CaCl ₂	0.8150	0.5095

TABLE II. β values for fits using Eq.13 for cations and anions in aqueous electrolytes.

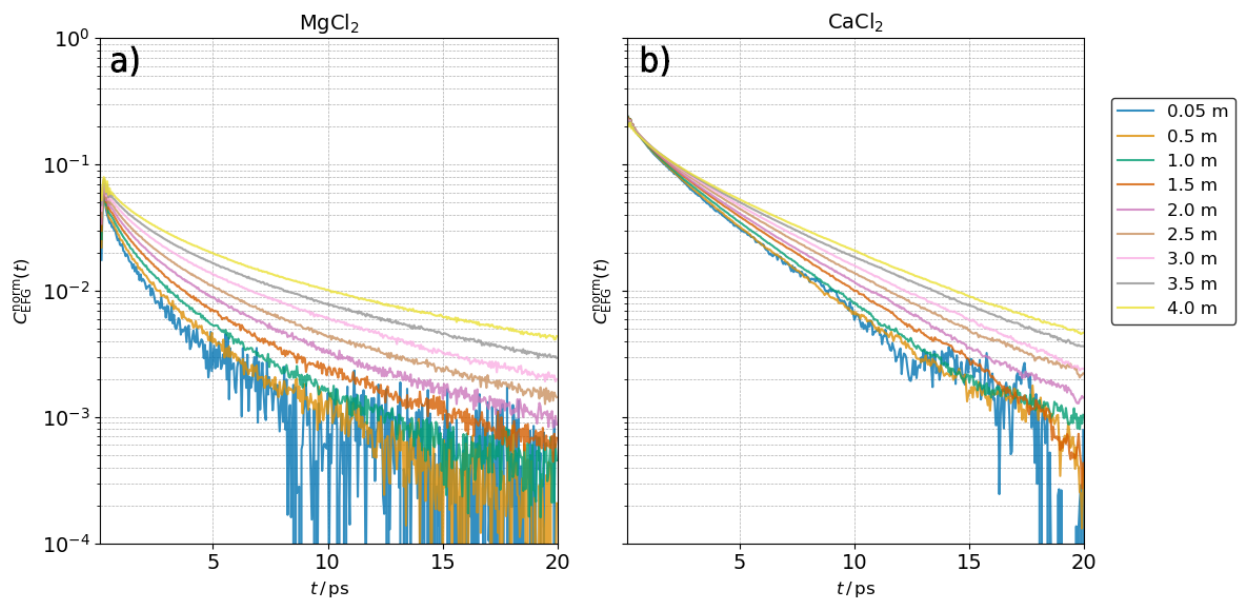


Fig. S2. Normalized autocorrelation function of the electric field gradient at the cation position for MgCl_2 , and CaCl_2 , as a function of time from 0 to 20 ps, presented for various molalities.

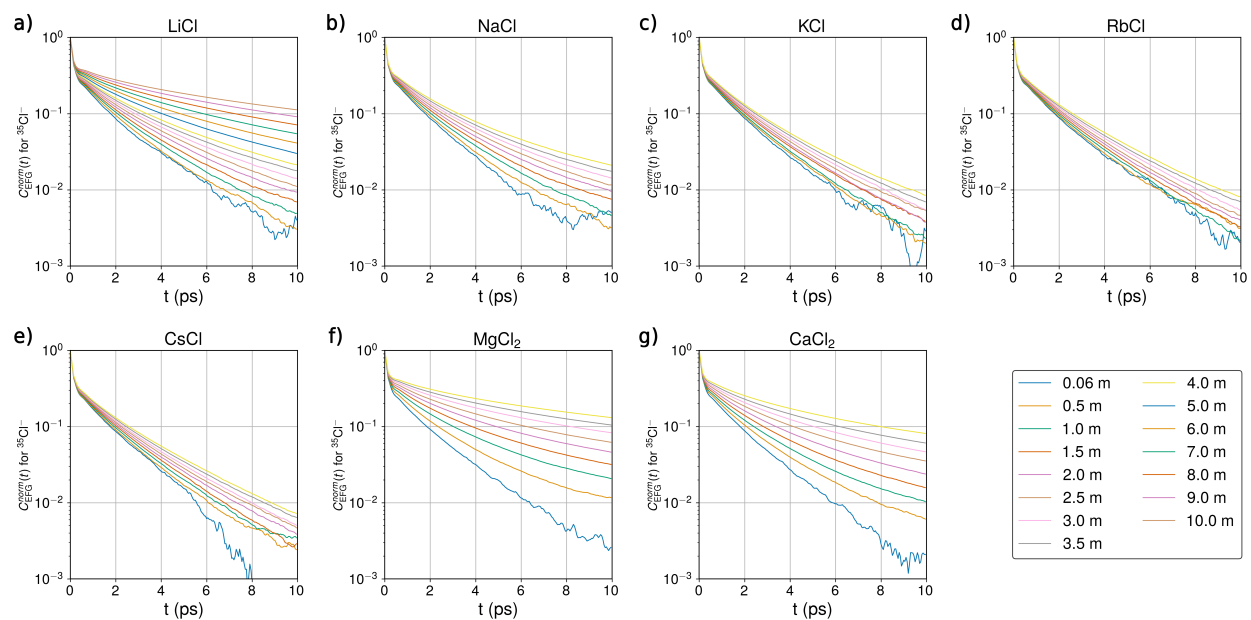


Fig. S3. Normalized autocorrelation function of the electric field gradient at the anion position in aqueous solutions of (a) LiCl , (b) NaCl , (c) KCl , (d) RbCl , (e) CsCl , (f) MgCl_2 , and (g) CaCl_2 , as a function of time, presented for various molalities indicated by the line colors.

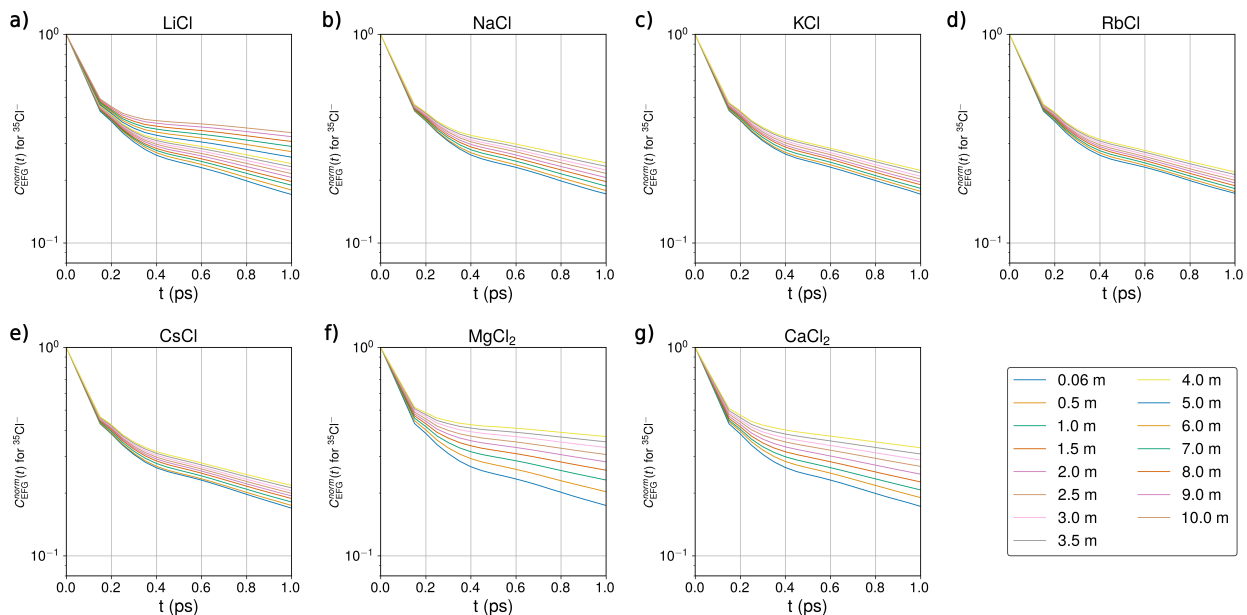


Fig. S4. Normalized autocorrelation function of the electric field gradient at the anion position in aqueous solutions of (a) LiCl, (b) NaCl, (c) KCl, (d) RbCl, (e) CsCl, (f) MgCl₂, and (g) CaCl₂, as a function of time, presented for various molalities indicated by the line colors.

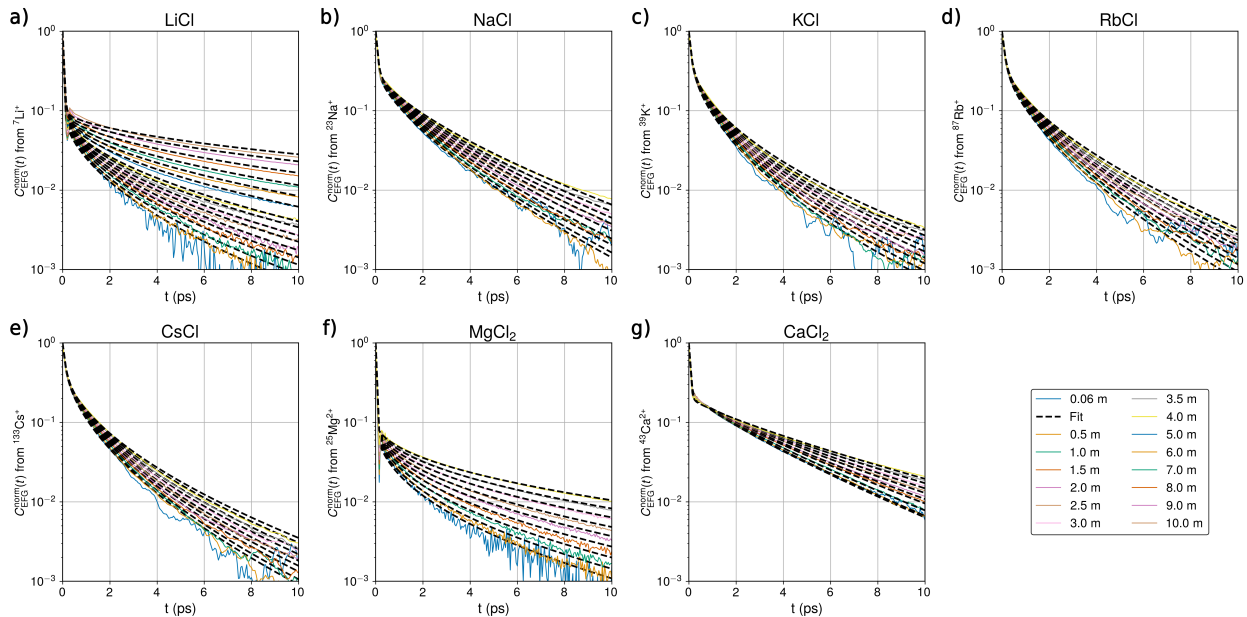


Fig. S5. Normalized autocorrelation function of the electric field gradient at the cation position in aqueous solutions of (a) LiCl, (b) NaCl, (c) KCl, (d) RbCl, (e) CsCl, (f) MgCl₂, and (g) CaCl₂, as a function of time for various molalities. The black dashed line represents a fit obtained using the following function: $f(t) = (1 - \alpha_s)e^{-t/\tau_f} + \alpha_s \cdot e^{-[t/\tau_s]^\beta}$.

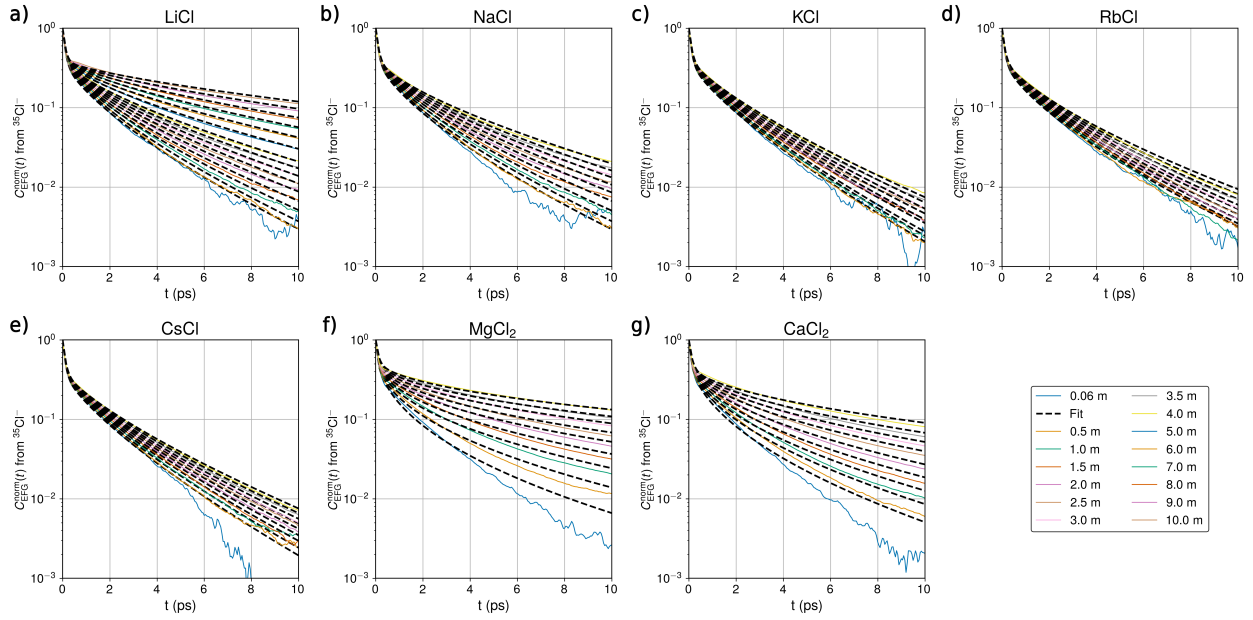


Fig. S6. Normalized autocorrelation function of the electric field gradient at the anion position in aqueous solutions of (a) LiCl, (b) NaCl, (c) KCl, (d) RbCl, (e) CsCl, (f) MgCl₂, and (g) CaCl₂, as a function of time for various molalities. The black dashed line represents a fit obtained using the following function: $f(t) = (1 - \alpha_s)e^{-t/\tau_f} + \alpha_s \cdot e^{-[t/\tau_s]^\beta}$.

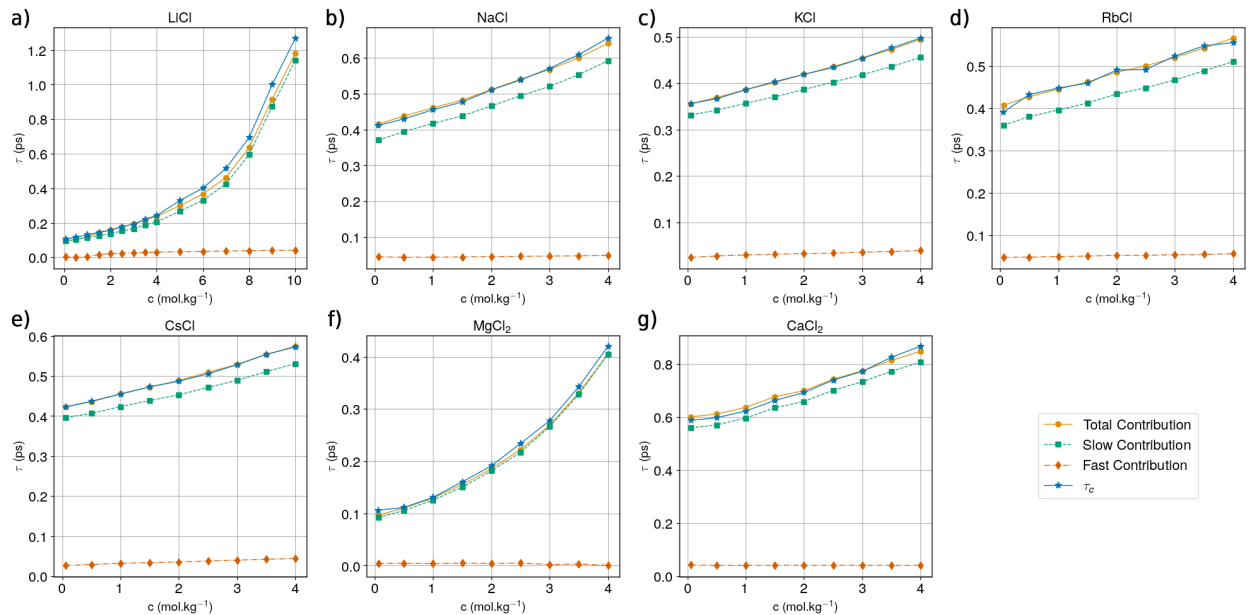


Fig. S7. The contribution of the fast and slow modes to the total EFG decorrelation time τ_c at the cation position was evaluated by integrating the following function: $f(t) = (1 - \alpha_s)e^{-t/\tau_f} + \alpha_s \cdot e^{-[t/\tau_s]^\beta}$, and extracting the respective contributions of the fast and slow modes.

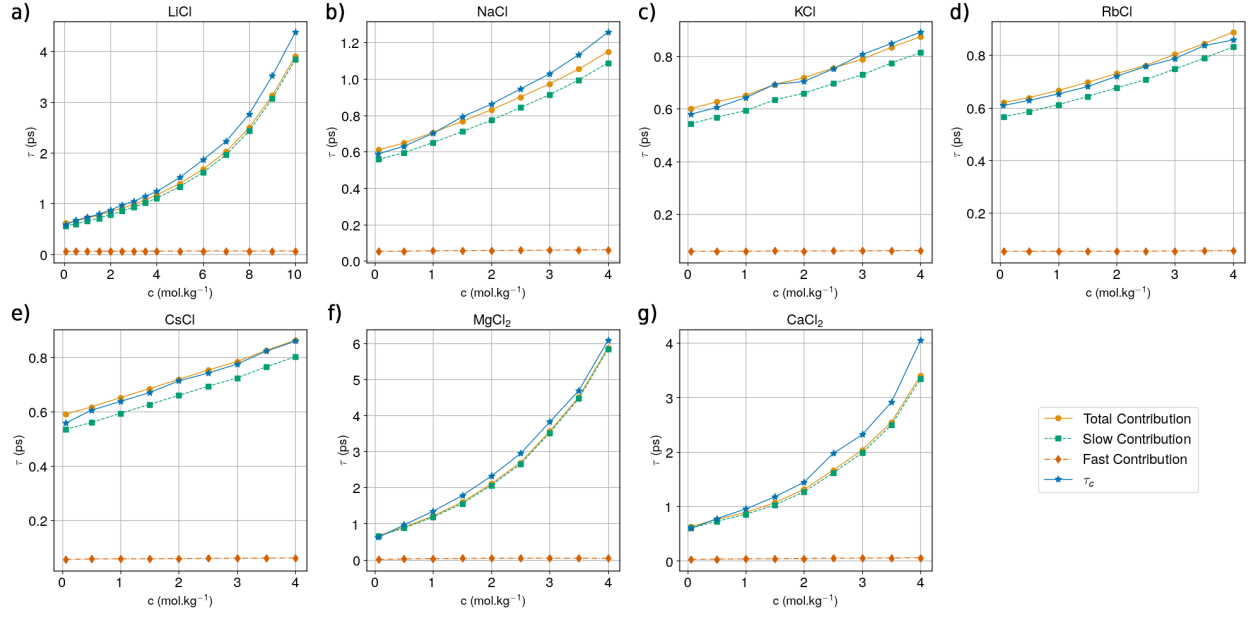


Fig. S8. The contribution of the fast and slow modes to the total EFG decorrelation time τ_c at the anion position was evaluated by integrating the following function: $f(t) = (1 - \alpha_s)e^{-t/\tau_f} + \alpha_s \cdot e^{-[t/\tau_s]^\beta}$, and extracting the respective contributions of the fast and slow modes.

Molality (m)	LiCl	NaCl	KCl	RbCl	CsCl	MgCl ₂	CaCl ₂
0.056	0.0189	16.58	14.26	611.29	0.1630	8.86	1.2473
0.5	0.0208	17.31	14.60	676.29	0.1681	9.33	1.2663
1.0	0.0232	18.28	15.33	699.53	0.1749	10.98	1.3153
1.5	0.0258	19.08	15.99	715.46	0.1815	13.50	1.3949
2.0	0.0280	20.38	16.57	763.96	0.1868	16.11	1.4480
2.5	0.0316	21.42	17.13	765.10	0.1936	19.76	1.5413
3.0	0.0342	22.63	17.87	812.83	0.2023	23.50	1.5987
3.5	0.0393	24.08	18.70	849.40	0.2119	29.07	1.6994
4.0	0.0433	25.85	19.49	860.74	0.2189	35.74	1.7710
5.0	0.0587	-	-	-	-	-	-
6.0	0.0719	-	-	-	-	-	-
7.0	0.0927	-	-	-	-	-	-
8.0	0.1254	-	-	-	-	-	-
9.0	0.1822	-	-	-	-	-	-
10.0	0.2326	-	-	-	-	-	-

TABLE III. Computed relaxation rates ($1/T_1$ in s^{-1}) for the different cations in all considered aqueous electrolytes as a function of the salt concentration at 25°C .

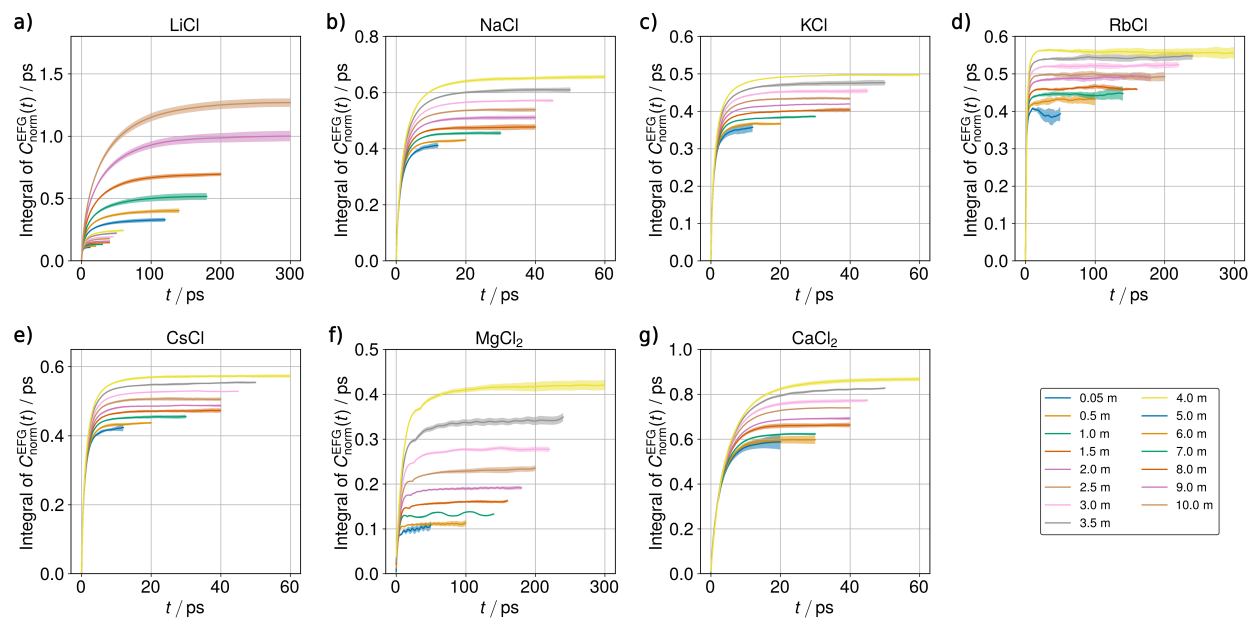


Fig. S9. Time-dependent integrals of the normalized EFG ACFs at the position of the different cations in aqueous solutions of (a) LiCl, (b) NaCl, (c) KCl, (d) RbCl, (e) CsCl, (f) MgCl_2 , and (g) CaCl_2 , as a function of time, presented for various molalities indicated by the line colours. The shaded region indicates the standard error over different simulation runs.

III. D.

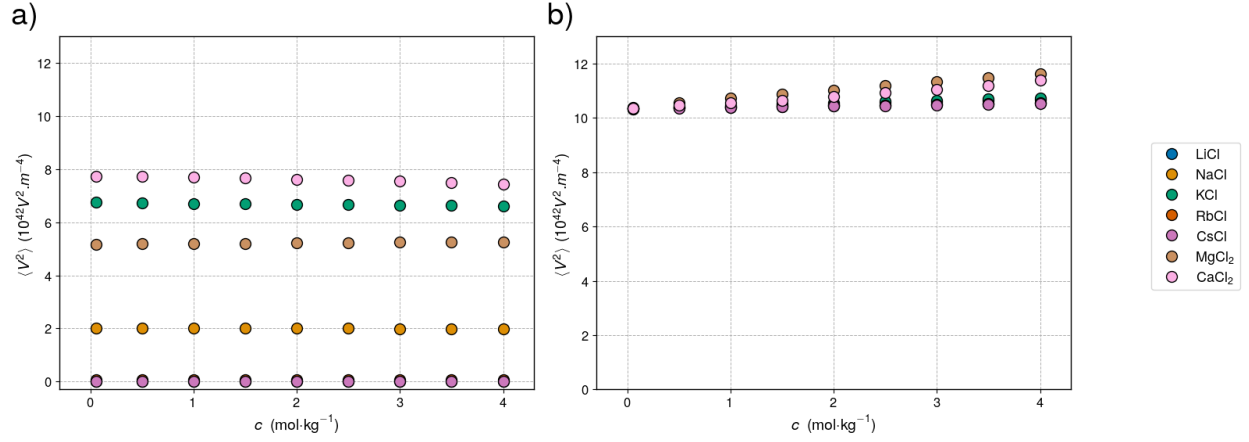


Fig. S10. Variance of the EFG at the cation position a) and anion position b) $\langle V^2 \rangle$ (including the effective Sternheimer factor) in aqueous (a) LiCl, (b) NaCl, (c) KCl, (d) RbCl, (e) CsCl, (f) MgCl₂, and (g) CaCl₂ solutions, as a function of molality.

III. F. 1.

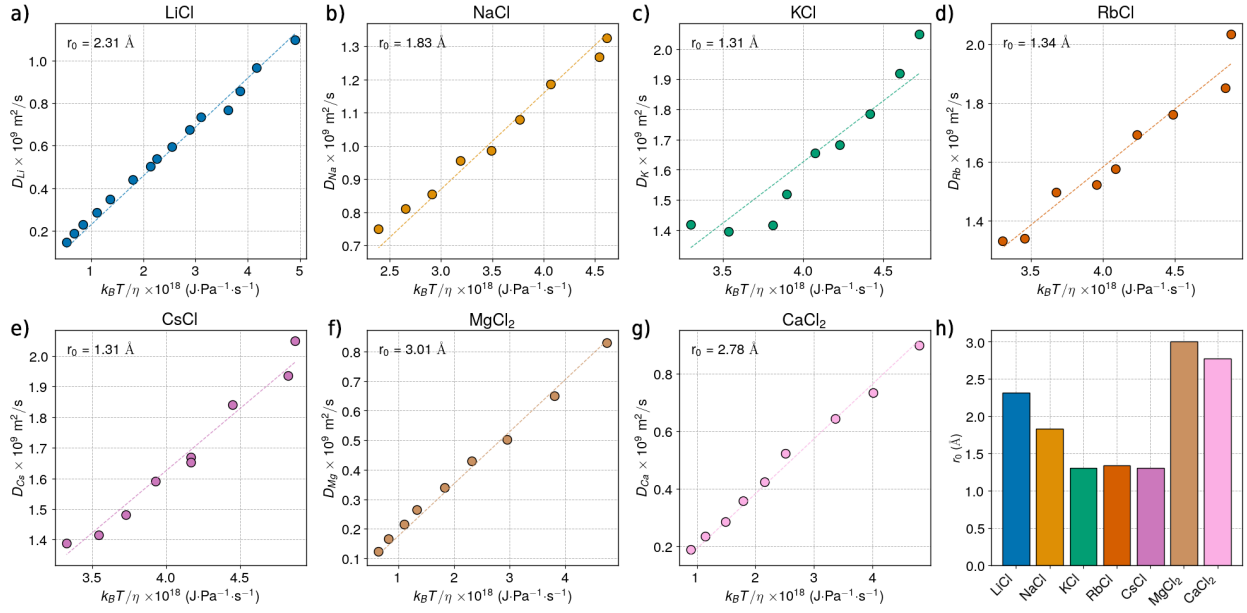


Fig. S11. Cation diffusion coefficients for various systems as a function of $k_B T / \eta$. For each system, the dotted line represents the fit of the data to the relation $D = k_B T / 6\pi\eta r_0$, with r_0 indicated in the top left corner of each plot and gathered in the final bar plot.

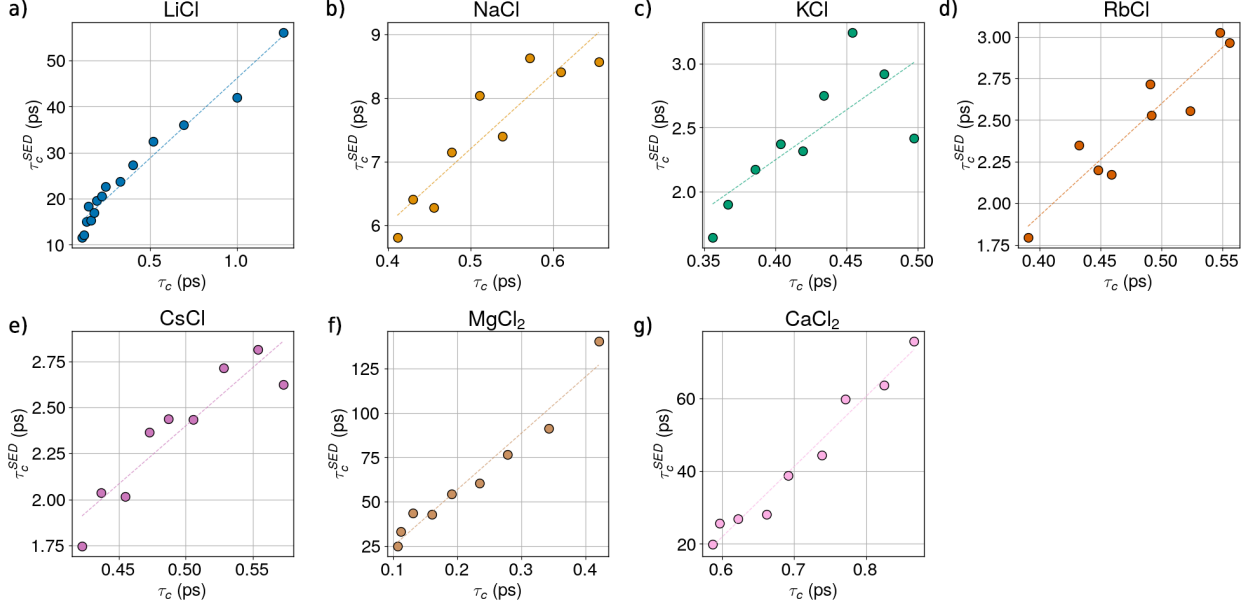


Fig. S12. Stokes-Einstein-Debye correlation times τ_{SED} for different ions in each system, as calculated from Equation 11, are plotted against the electric field gradient (EFG) at the position of the cation from each system represented correlation times τ_c extracted from simulation data at various molalities. The grey dotted line represents a linear fit for visual guidance.

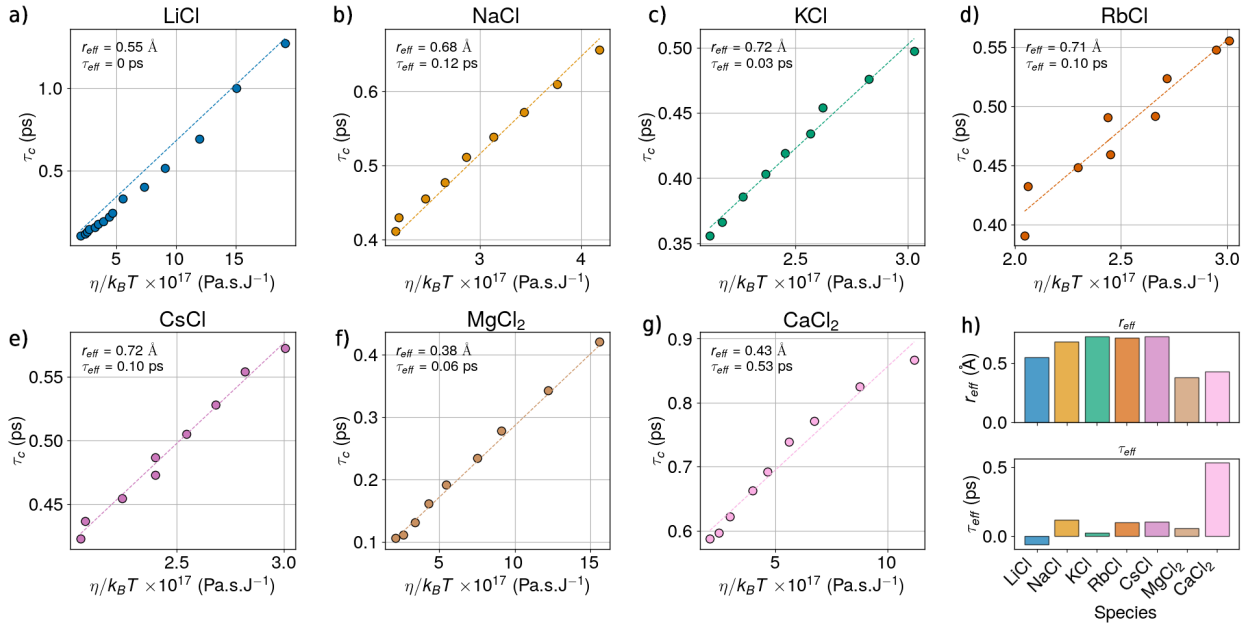


Fig. S13. For the different ions of each system, τ_c is plotted versus $\eta/k_B T$ at different molalities. The dotted lines show the fit from the equation 14 with the best-fit parameters r_{eff} and τ_{eff} indicated in the top corner left of each figure.

III. F. 2.

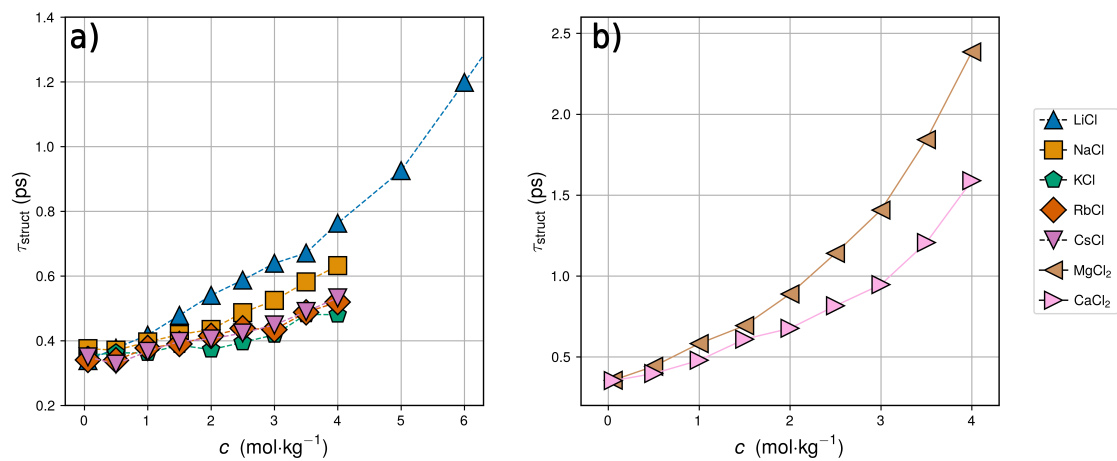


Fig. S14. Structural relaxation time τ_{struct} as a function of molality, for aqueous alkali metal chlorides (left) and alkaline earth chloride (right) solutions. The nature of the cation is indicated by the color and dashed lines are only guides for the eyes.